People's Democratic Republic of Algeria
Ministry of Higher Education and Scientific Research
Kasdi Merbah University of Ouargla
Faculty of New Information and Communication Technologies
Department of Electronics and Telecommunications

Academic Master's thesis

Domain: Science and technology
Sector: Telecommunications
Option: Telecommunications System

Presented by:

•Trabelsi hibat
•Bougossa Hadjer

Theme:

Intelligent Reflecting Surfaces in Massive MIMO Systems

In front of the jury:

Mr. Moad Mohamed Sayah	Président	MCA, KMU Ouargla
Mdm. Benkrinah Sabra	Examiner	MCB, KMU Ouargla
Mr. Aounallah Naceur	Supervisor	Professor, KMU Ouargla
Mr. Labed Smail	Co-Supervisor	PhD student, KMU Ouargla

Academic Year: 2024/2025


بسم الله الرحمن الرحيم

Acknowledgement

*First of all, all thanks and praise to our almighty God **'ALLAH'** for giving us the courage, the will, and the patience to complete this present work.*

*We extend our sincere thanks to our supervisor, **Prof. AOUNALLAH Naceur**, who provided us with valuable advice and suggestions. We are also grateful for the opportunity to benefit from his scientific skills.*

*We also extend our sincere thanks to **Dr. LABED Ismail** for his supervision and support during the completion of this work, and we are grateful for his encouragement and valuable advice.*

*We extend our sincere gratitude to the members of the **jury** committee for accepting to read and evaluate this modest work.*

We extend our sincere thanks to all the professors who contributed to our training in the Electronics and Communications Department.

We extend our sincere thanks to the **Trabelsi** *and* **Bougossa** *families for their moral and financial support throughout the preparation period.*

*Finally, we extend our sincere thanks to our **friends** and everyone who contributed, directly or indirectly, to the completion of this work.*

Thank you all 

DEDICATIONS I

To my father, ***Abdel Naceur:*** *I cannot find the words to describe all the love I feel for you. Your constant concern for our safety, your blessings, your prayers, your courage, and your support have brought me here today. I dedicate this work to you. May God prolong your life and protect you for us.*

To my ***mother****, you are my most precious possession and my guardian. You devoted all your time to raising me from a young age. This work is the beginning of my recompense for your many sacrifices. I will never be able to repay you for your kindness. Thank you for who I am today. May God protect you for us, prolong your life, and grant you health and wellness.*

To my dear sisters, ***Houda, Zinab****, and* ***Ikhlas****; to my brother* ***Salah*** *and his wife* ***Amina****; to my nieces* ***Dareen*** *and* ***Anas****; and to my niece* ***Sidra****. Your support and assistance have never let me down; you have been a source of pride throughout my studies.*

To my beloved ***Hadjer****, who shared my arduous journey and supported me during moments of failure and fatigue. Thank you for standing by me.*

*To my friends, companions, and the best people I have known (****Nour Al Houda, Hanane****, and* ***Zahra****), thank you for all the support and encouragement you have given me throughout my life and academic journey. I also thank you for standing by me during the most difficult times. And for all these years of friendship, which we hope will continue for a long time to come.*

who loves me and whom I love.

Hiba 

DEDICATIONS II

Praise be to God, Lord of the Worlds, and peace and blessings be upon the Seal of the Prophets and Messengers.

I dedicate the fruit of this work to the One whom the Most Merciful has commanded and enjoined obedience to.

To the first person my eyes have seen, the dearest to my heart, the first person I have embraced, the one I rejoice in seeing and find comfort in meeting, my school in life, the one who rejoices in my success and encourages me at every step, to my ***"beloved mother"***

To the one who raised me with noble morals, taught me to love work, helped me chart the path to success and love God, and has been my support throughout my life. To the one whose name is exalted and whose value is elevated, ***"my dear father"*** *May God protect him and prolong his life.*

To those for whom I have sincere love, loyalty, and compassion; to those with whom I am united by the darkness of kinship, who have been my support throughout my academic journey—my ***brothers*** *and* ***sisters****. May God grant them success and guide their steps.*

To the one who taught me the meaning of friendship and shared this work with me I hope God never separates us: ***"Hiba"***

To all my ***friends*** *and* ***relatives****, and to the second-year MA students in media, I wish them success in their studies.*

To everyone who has held an ounce of love and affection for me in their hearts.

Hadjer 

Abstract To improve wireless communications performance, this study focuses on integrating intelligent reflective surfaces (IRS) into massive MIMO systems. IRSs are emerging as a promising solution for managing the wireless propagation environment, given the increasing demands for high data rates, energy efficiency, and reliable connectivity in networks ranging from 4G to 6G. The main objective of this work is to evaluate the effectiveness of IRSs in improving the performance of massive MIMO systems by increasing spectral efficiency, reducing interference, and improving signal quality. Simulation results show that systems incorporating IRSs significantly outperform conventional MIMO and relay-based systems, particularly in non-line-of-sight (NLOS) scenarios. Algorithms such as DS-OMP offer efficient methods for channel estimation. The adoption of advanced technologies such as IRSs is essential to meet the future demands of wireless communications.

Keywords: IRS, massive MIMO, 4G, 5G, and 6G wireless networks, path loss, relay, energy, Energy efficiency, channel estimation.

Résumé Pour améliorer les performances des communications sans fil, cette étude se concentre sur l'intégration des surfaces réfléchissantes intelligentes (IRS) dans les systèmes MIMO massifs. Les IRS apparaissent comme une solution prometteuse pour gérer l'environnement de propagation sans fil, face à l'augmentation des besoins en débits élevés, en efficacité énergétique et en connectivité fiable dans les réseaux allant de la 4G à la 6G. L'objectif principal de ce travail est d'évaluer l'efficacité des IRS dans l'amélioration des performances des systèmes MIMO massif, en augmentant l'efficacité spectrale, en réduisant les interférences et en améliorant la qualité du signal. Les résultats de simulation montrent que les systèmes intégrant des IRS surpassent nettement les systèmes MIMO classiques et ceux basés sur des relais, en particulier dans les scénarios sans ligne de vue directe (NLOS). Des algorithmes comme DS-OMP offrent des méthodes efficaces pour l'estimation du canal. L'adoption de technologies avancées telles que les IRS est essentielle pour répondre aux exigences futures des communications sans fil.

Mots-clés: IRS, MIMO massif, réseaux sans fil 4G, 5G et 6G, perte de propagation, relais, efficacité énergétique, estimation de canal.

ملـخــص:

لتحسين أداء الاتصالات اللاسلكية، تركز هذه الدراسة على دمج الأسطح العاكسة الذكية (IRS) في أنظمة MIMO Massive.

تبرز أنظمة IRS كحل واعد لإدارة بيئة الانتشار اللاسلكي، في مواجهة الاحتياجات المتزايدة لمعدلات البيانات العالية وكفاءة الطاقة والاتصال الموثوق به في الشبكات التي تتراوح من 4G إلى 6G. الهدف الرئيسي من هذا العمل هو تقييم فعالية IRS في تحسين أداء أنظمة MIMO الضخمة، من خلال زيادة الكفاءة الطيفية وتقليل التداخل وتحسين جودة الإشارة. تظهر نتائج المحاكاة أن الأنظمة التي تتضمن IRS تتفوق بشكل كبير على أنظمة MIMO التقليدية والأنظمة القائمة على التتابع، وخاصة في سيناريوهات عدم خط البصر (NLOS). توفر الخوارزميات مثل DS-OMP طرقًا فعالة لتقدير القناة. إن اعتماد التقنيات المتقدمة مثل IRS أمر ضروري لتلبية متطلبات الاتصالات اللاسلكية المستقبلية.

الكلمات المفتاحية:

الأسطح العاكسة الذكية، الهوائيات الضخمة، شبكات الجيل الرابع والخامس والسادس اللاسلكية، فقدان الانتشار، المرحلات، كفاءة الطاقة، تقدير القنوات.

Contents

List of Figures

List of Tables

List of Symboles

1G: first generation.
2G: second generation.
3G: third generation.
4G: fourth generation.
5G: fifth generation.
5GC: 5G Core network.
6G: Sixth generation.
3GPP: 3rd Generation Partnership Project.
AWGN: additive white Gaussian noise.
AI: artificial intelligence.
AoA: angles of arrival.
AoD: angles of departure.
AF: Amplify and forward.
BS: base station.
CSI: Channel State Information.
CogRF: Cognitive Radio radio frequency.
CR: Cognitive Radio.
CB: conjugate beamforming.
CS: compressive sensing.
CDMA: Code Division Multiple Access.
DBF: Digital beamforming.
DAC: digital-to-analog converter.
DRL: Deep reinforcement learning.
DL: Downlink.
DF: decode and forward.
DCS: digital steerable hubs.
D2D: device-to-device.
DFT: Discrete Fourier Transform.

DS-OMP:	double-structured orthogonal matching pursuit.
E-UTRAN:	Evolved Universal Terrestrial Radio Access Network.
eMBB:	Enhanced Mobile Broadband.
EPC:	Evolved Packet Core.
FDD:	Frequency Division Duplexing.
GS:	Gauss-Seidel.
GPS:	global positioning system.
HSS:	Home Subscriber Server.
HAPS:	high-altitude platform stations.
IP:	Internet Protocol.
IoT:	Internet of Things.
IEEE:	Institute of Electrical and Electronics Engineers.
IRS:	Intelligent Reflecting Surface.
LTE:	lone term evolution.
LTE Advanced:	lone term evolution- Advanced.
LOS:	line-of-sight.
LS:	least squares.
LIS:	large smart surfaces.
MIMO:	multiple-input, multiple-output.
mMIMO:	Massive multiple-input, multiple-output.
MF:	Matching filter.
MMSE:	Minimum Mean Squared Error.
MME:	Mobility Management Entity.
MmWave:	Millimeter wave.
ML:	machine learning.
MEC:	Mobile Edge Computing.
MRT:	Maximum Ratio Transmission.
MU-MIMO:	Multi-User MIMO.
NR:	New Radio.
NLOS:	non line-of-sight.
NG RAN:	next-generation radio access network.
NMSE:	Normalized Mean Squared Error.

OFDM: Orthogonal frequency-division multiplexing.
OAM: orbital angular momentum.
OMP: orthogonal matching pursuit.
PDN: PDN Gateway.
PGW: Packet Data Network Gateway.
PDU: Protocol Data Unit.
QoS: quality of service.
RF: Radio frequance.
RIS: Reconfigurable Intelligent Surfaces
RRH: radio head unit.
SNR: signal-to-noise ratio.
SE: spectral efficiency.
SD: spherical decoder.
SBA: service-based architecture.
SMF: Session Management Function.
SGW: Serving Gateway.
SS-OMP: Structurally Sparse orthogonal matching pursuit.
SISO: Single Input Single Output.
TCP: Transmission control protocol.
TDD: Time Division Duplexing.
UE: user equipment.
USPA: uniform square planar array.
UAV: Unmanned aerial vehicle.
UL: uplink.
UMTS: Universal Mobile Telecommunication System.
WiMAX: Worldwide interoperability for microwave access.
ZF: zero-forcing.

General Introduction

The rapid development of mobile communications from the fourth generation (4G) to the sixth generation (6G) has enabled comprehensive connectivity, higher spectrum efficiency, and high-speed data transmission. The increasing use of mobile devices and the increasing requirements for quality and performance have challenged traditional systems. This has led to the development of massive MIMO technology, which uses multiple antennas to increase capacity, reduce interference, and amplify signals. In particular, beamforming, channel prediction, and energy efficiency still pose significant challenges.

Therefore, by passively and intelligently controlling the propagation of electromagnetic waves, intelligent reflective surfaces (IRS) have been investigated as a novel way to enhance massive MIMO systems. The structure, kinds, real-world uses, and integration of IRS technology with MIMO technologies are all thoroughly examined in this study. This sheds light on how the IRS can enhance wireless communications in the future. The influence and function of IRS technology in enhancing massive MIMO systems' performance in contemporary wireless networks are examined in this research, with an emphasis on how it might be able to overcome present obstacles. This study consists of three chapters:

Chapter 1 introduces the evolution from the fourth generation (4G) to the sixth generation (6G) networks, focusing on the current MIMO technology and its impact on each generation.

Chapter 2 introduces the concept, structure, types (passive and active), applications, and role of IRS systems in improving the performance of wireless networks. It also discusses the technical challenges of these networks.

Chapter 3 analyzes and compares IRS-based systems with traditional systems such as SISO and DF-Relay and simulates their performance using metrics such as channel capacity, surface area, energy efficiency, path loss, and power consumption.

Chapter 1

Communication networks from 4G to 6G and modern MIMO technologies

1.1 Introduction

This chapter focuses on the transition from the fourth generation to the sixth generation of wireless networks, which are evolving from the first generation to the sixth. Every generation adds new features to improve network efficiency, data throughput, access time, and connection by addressing the shortcomings of earlier generations. It discusses the key challenges faced by these technologies, the benefits of each generation in contemporary communication networks, and the significance of advanced MIMO technologies in each generation.

1.2 Evolution of Wireless Communication Systems

The early 1980 marked the beginning of the era of mobile communications, which has witnessed significant growth in the past few decades. From 1G to 5G and beyond, cellular networks have evolved over time. Base stations, user devices (phones), and core networks make up any cellular network. The evolution from 1G to 6G is summarized in FIGURE1.1 [1].

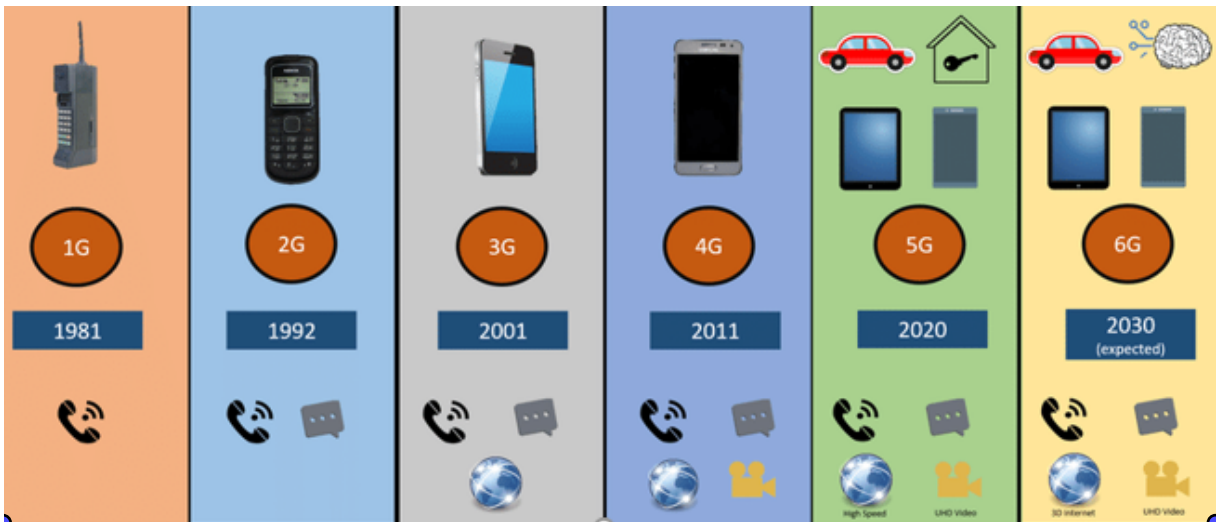

Figure 1.1: The evolution of mobile communication 1G to 6G.

1.2.1 The fourth generation (4G)

The 4G of mobile broadband, was first released in 2010. The new LTE standard, on which it is based, offers fast data transmission rates and a bandwidth of $100Mb/s$ for mobile operations and $1Gb/s$ for fixed operations. It is growing globally and can send video and audio data within a cell over up to $100kilometers(62mi)$. Advanced wireless

technologies like MIMO and OFDM are used in 4G networks, which include WiMAX, LTE, and LTE-Advanced. Some of the significant advantages of 4G are [2]:

1. **Pure Data Network:** More bandwidth is possible with a pure data network, allowing for the transmission of more data via Internet Protocol.
2. **More Devices and Applications:** By utilizing the bandwidth and faster speeds, 4G network devices can provide more potent data applications.
3. **Speed:** The theoretical speed of the 4G network has been suggested with data rates of up to 100*Mbps* for high mobility and 1*Gbps* for low mobility being the target value.
4. **Handover:** The upgraded 4G network standards will allow seamless handover from one coverage region to another without disrupting any ongoing data transfers.
5. **Faster Response Time:** 4G technology offers the advantage of reduced latency or faster response time. Latency is reduced to 1/100 of a second (about 10*milliseconds*) with 4G technology.

1.2.1.1 Network Architecture of 4G

The e-UTRAN (Evolved Universal Terrestrial Radio Access Network), which is the access network, and the EPC (Evolved Packet Core), which is the network's core, make up the general architecture of the LTE network [3].
The LTE access network is called e-UTRAN and is composed of :

- **The UE (user equipment: smartphone, laptop, etc.):** In LTE, the UE communicates with the e-UTRAN and the EPC using protocols.
- **e-NodeB:** The eNodeB is responsible for radio transmission and reception with the UE.

The main tenets of the EPC are:

- SGW stands for Serving Gateway.
- PDN Gateway (PGW).
- Mobility Management Entity, or MME.
- Home Subscriber Server, or HSS.

When a user wants to browse the Internet, they must register on the LTE network using a process known as ”Network attachment.” The UE connects to the ”eNodeB” antenna, which transmits the request to the MME. Initially, the HSS server authenticates the user. The MME then sends a session request, which SAEGW receives and uses an IP address that is available. The SAE-GW will provide the MME with the session's response, and the MME will provide the UE with all of the information [3].

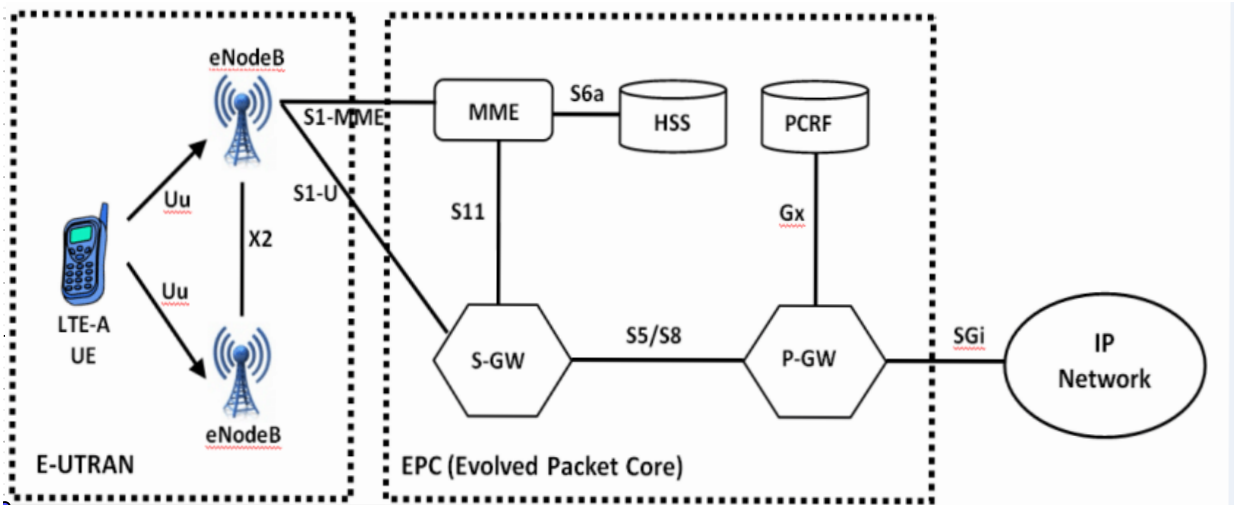

Figure 1.2: LTE architecture

MIMO systems are an essential part of LTE in order to meet the ambitious requirements for throughput and spectrum efficiency. MIMO refers to the use of multiple antennas on both the transmitter and receiver side [4].

1.2.1.2 MIMO in 4G technology

MIMO is a wireless technology that uses additional receivers and carriers to transmit more data at the same time. Different transmission methods are used using multiple ”smart” receivers in addition to ”space” crossing to greatly improve performance and gateway. MIMO allows multiple antennas to transmit and receive simultaneous spatial streams simultaneously. Antennas can also be grouped and allowed to broadcast data from multiple links to increase the efficiency of the received signal. Spatial diversity technology allows it to take advantage of the best properties of non-standard antennas, and additional antennas can add diversity to receivers through increased diversity and continuous broadcasting [5].

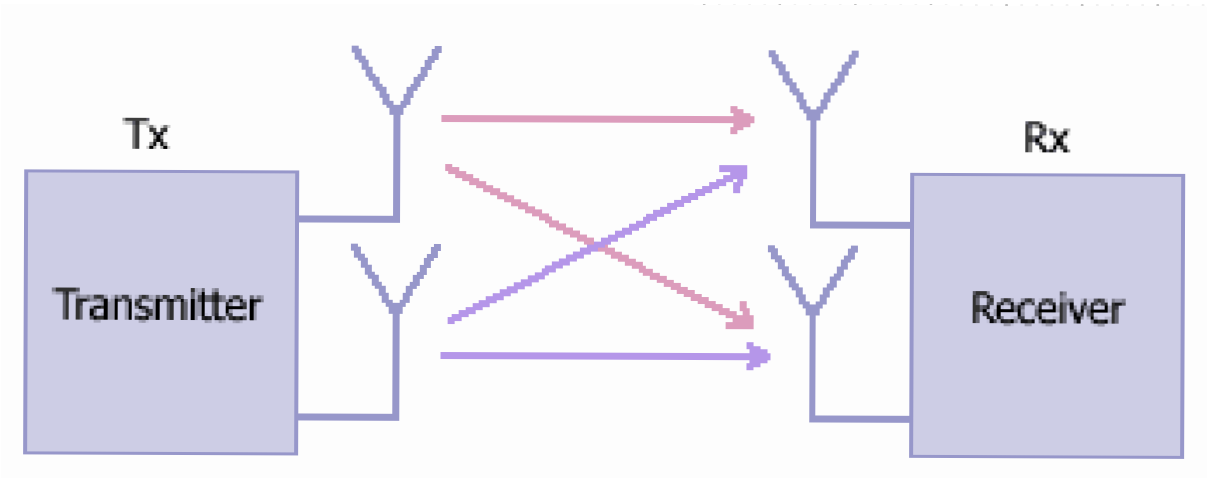

Figure 1.3: MIMO 2 × 2 systems

MIMO also offers other benefits through spatial multiplexing and spatial diversity and beamforming.

A) Spatial Multiplexing:

Spatial multiplexing (SM) is an important feature of MIMO (multiple-input, multiple-output) that increases data rate by dividing the outgoing signal stream into multiple parts that are transmitted simultaneously and in parallel on the same radio frequency channel via multiple spatially separated antennas on both the transmitter and receiver [6].

Spatial multiplexing is effective in high signal-to-noise ratio systems and bandwidth-limited radio networks. Multiple spatial streams require adequate channel variance. However, spatial multiplexing is ineffective in low signal-to-noise ratio operating environments, where the transmitter must divide the power into multiple streams to effectively increase capacity without requiring additional bandwidth or power [4].

B) Spatial diversity (SD):

Spatial diversity is about improving the quality of a wireless signal by using multiple transmissions to address the negative impact of multipath fading. One of the benefits of using MIMO is antenna diversity and the ability to diversify or split the signal either at the transmitter end or the receiver end. To mitigate the risk of signal fading [7].

C) Beamforming:

In beamforming, multiple antennas send the same signal toward the intended user rather than broadcasting it in all directions to expand the signal range, improve bit rates and signal strength, and reduce interference with other users. Beamforming is one of

the key benefits of MIMO and is a user-friendly technology for 5G New Radio (NR) networks [6].

1.2.2 The fifth generation (5G)

5G is the new generation that entered the market in 2019 and will be commercially launched in 2021. It is one of the latest cellular technologies in mobile phones and has evolved in mobile communication standards in line with the current 4G LTE (Long Term Evolution) standard. To respond to the needs of the population, it has an extraordinary data transmission capacity thanks to massive MIMO systems. It also provides unlimited call volumes, a large additional discount, and a download waiting time of up to $1 millisecond$. According to the relationship with the quad-generation, it took 10 days longer [8].

5G devices operate within multiple bands from 3 to $300 GHz$.low-frequency games at $6 GHz$ and dense bands from 30 to $300 GHz$ are used for different millimeters [9].

5G enables faster connections and downloads than other generations. It therefore aims to:

- At the edge of the cell, 5G technology offers $1,000$ times faster data rates and a wider coverage area.
- Lower response time compared to LTE.
- Ensure you have a fast internet connection on your smartphone.
- Capacity compared to the higher 4G network.
- Sensors can communicate wirelessly with multiple devices at once and consume less power.
- Data transfer rates of up to about $1 Gb/s$ can be easily achieved, and energy and spectral efficiency are good [9].

1.2.2.1 Network Architecture of 5G

Prior to the introduction of 5G, the design of cellular network architecture was centered on end users. Cellular network designers aimed to provide increased capacity from generation to generation, evolving the infrastructure into a full IP architecture, as seen in 5G. As shown in Figure1.4.

The 5G network is made up of two primary parts: the 5G access network (AN) and the 5G core network. The access network is made up of a next-generation radio access network (NG RAN) that communicates via the 5G New Radio (NR) interface. The various network entities are linked via the TCP/IP backbone, which enables QoS profiles [10].

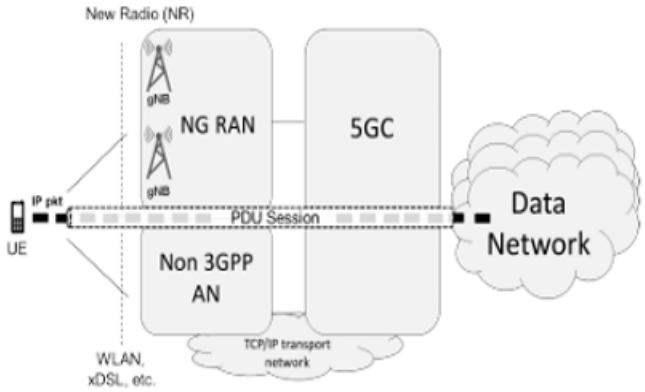

Figure 1.4: 5G Network Architecture

1- The next generation wireless access network (NG-RAN):

Is made up of gNBs, or 5G base stations, that connect to the 5GC network via logical interfaces (see figure 1.5). The gNBs can connect to one another via the X_n interface, which is linked to the NR interface. The gNBs architecture is divided into:

The central unit (gNB-CU): Which manages the basic control and data processing, and is divided into two parts. The first part for control plane functions (gNB-CU-CP), and the second part for user plane functions (gNB-CU-UP). As shown in Figure1.5.

The unit (gNB-DU): Connected to the remote radio head unit (RRH), which sends and receives signals between the base station and the user, amplifies the signals before sending them to the antennas, and has other functions [10].

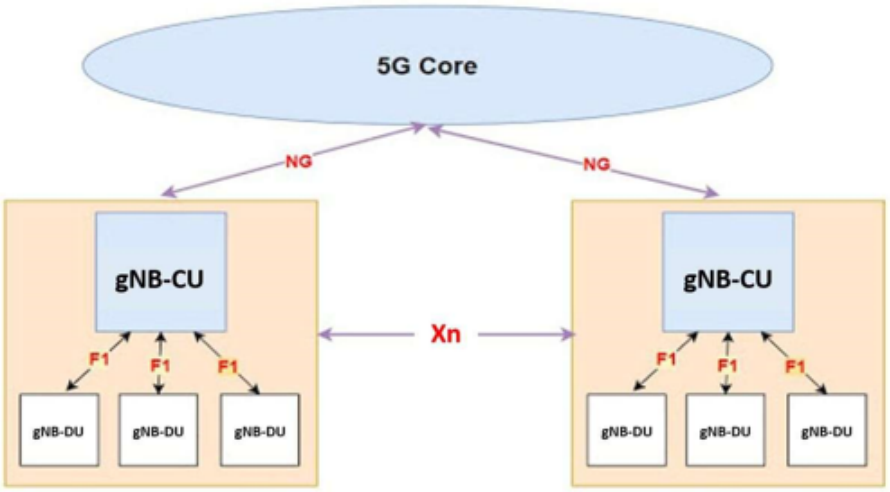

Figure 1.5: NG-RAN Architecture

2- The 5G core network (5GC):

The 3rd Generation Partnership Project (3GPP) defines the 5GC design as a service-based architecture (SBA) made up of numerous unified elements known as network functions (NFs). To boost performance and scalability, the core network is divided into two parts: the control plane and the user plane. At the user plane, we have one or more user plane functions (UPFs), which are primarily responsible for packet forwarding across different NG-U tunnels that compose a PDU session. All additional network functions are part of the control plane (CP) [11].

5G Network Functions:

a. AMF (Access and Mobility Management Function): Responsible for all 5GC signaling, i.e. providing functions such as access control, registration, and mobility management. Session management functions are provided by SMF.

b. SMF (Session Management Function): It also provides support for assigning IP address to UE and configuring routing decisions in UPF to facilitate routing traffic to appropriate destinations. Another important function of UPF is that it connects to the data network, known as the Protocol Data Unit (PDU) session anchor.

c. PDU (Protocol Data Unit): represents a 5G communication channel service, consisting of a series of NG tunnels to transmit data between the user device and the core network or its 5GC control functions, as well as to the external data network

to exchange user traffic. The PDU session is also divided into several QoS streams according to the data type (video, calls, etc.).

d. PCF (Policy Control Function): It is a unified entity that provides rules (QoS, filtering, loading, etc.).

e. UDM (Unified Data Management): Provides user identification function and generates authentication credentials. UDM also supports SMS management and subscription.

f. AUSF (Authentication Server Function): Supports authentication for 3GPP and other accesses.

j. NSSF (Network Slice Selection Function): Determines the network capabilities and network events of the UE. It is usually part of AMF [11].

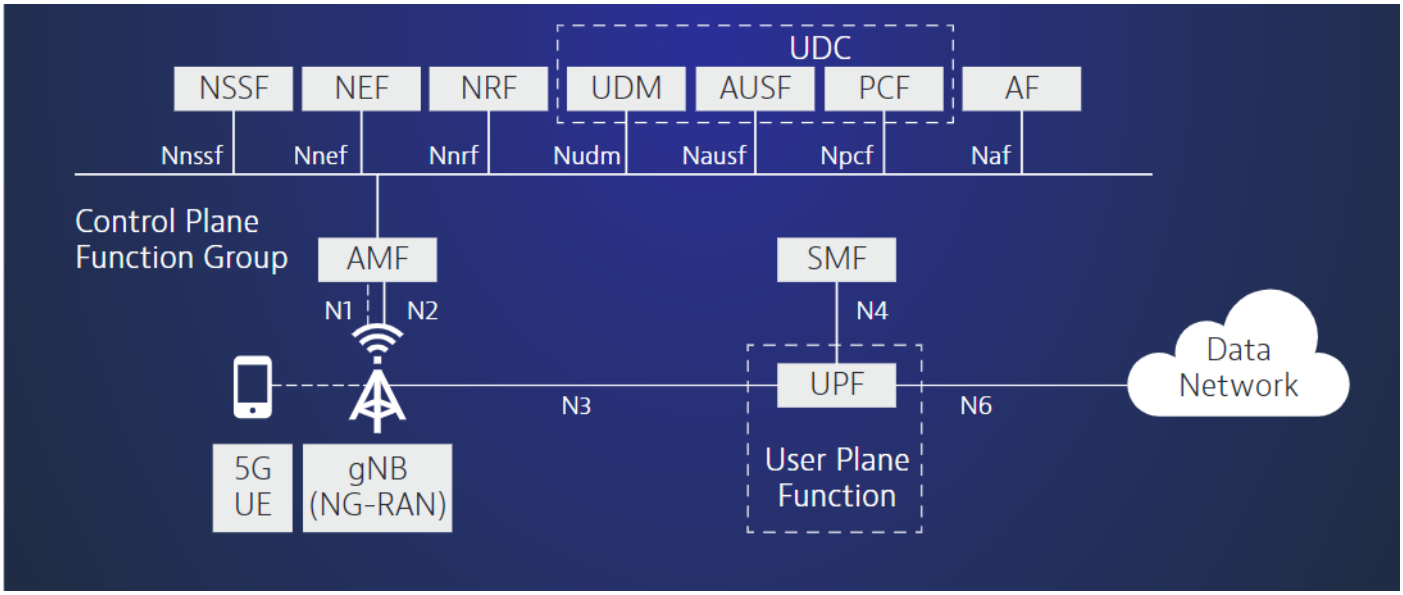

Figure 1.6: 5G core network Architecture

1.2.2.2 Millimeter Wave

Millimeter wave (*mmWave*) is one of the most promising technologies in 5G networks, with high data transfer rates that satisfy the needs of this generation. Their wavelengths, which range from 1 to 10*mm*, are far shorter than those utilized in modern wireless communication systems, therefore their name. Millimeter wave technology is based on a high-frequency range of 30 to 300*GHZ*. However, many studies and experiments are looking at frequencies above 6*GHZ* and beyond this range. As shown

in Figure 1.7, the wide bandwidth provided by these waves makes it possible to achieve fast data transfer rates. This noise-free approach works best in crowded environments and with the transmitter and receiver in direct line of sight. This gives millimeter wave several advantages, which include high bandwidth availability and resistance to exposure to microwave radiation. However, millimeter waves also have drawbacks such as low wall penetration, short range, low propagation angles, and strong absorption by airborne particles. [12].

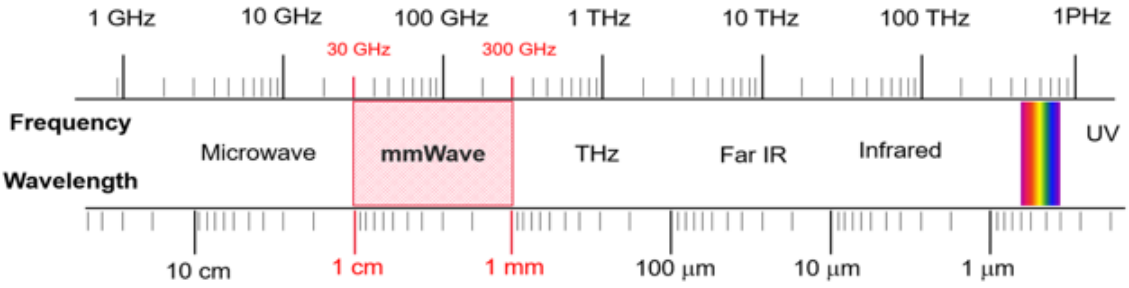

Figure 1.7: Schematic Diagram of Millimeter Wave Frequency Band.

Frequency bands allocated for mmWave in 5G NR

The Third Generation Partnership Project (3GPP) identified two frequency ranges that comprised the suitable spectrum for 5G NR. As part of the First Frequency Range (FR1), the sub-6GHz frequency band is located between 450MHz and 6GHz , Ideal for moderate speeds and broad coverage. Second, or FR_2 ($mmWave$), is the frequency range of 24.25GHz to 52.6GHz has a short range yet offers extremely high speeds [13].

1.2.2.3 Massive MIMO in 5G

Massive MIMO (multiple-input, multiple-output) is an evolution of traditional MIMO systems used in current wireless networks, as depicted in the figure 1.8, that combines hundreds or even thousands of antennas in a base station equipped with large-area antenna arrays to serve dozens of users at the same time [14]. The base station is capable of sending numerous independent data streams to customers. It can also deliver signals in multiple spatial directions, so increasing network capacity, reducing interference, and increasing data transfer rates [15]. In general, massive MIMO technology plays a crucial role in 5G technology by:

- **Increasing capacity and link:** Massive MIMO technology increases diversity gain, providing link strength with resistance to fading. It also allows a much larger number of users to connect to the network and use data at the same time.

- **Spectral efficiency:** Massive MIMO technology improves the spectral efficiency (SE) of a cellular network by spatially transporting a large number of user devices per cell. Higher throughput, thus achieving high spectral efficiency.
- **Improved signal coverage:** Provides better signal coverage, especially in areas with weak signals, ensuring stable communication.
- **Power efficiency:** Thanks to the coherent structure, the transmitted power is inversely proportional to the number of transmitting antennas. As the number of transmitting antennas increases, the transmission power decreases significantly [16].

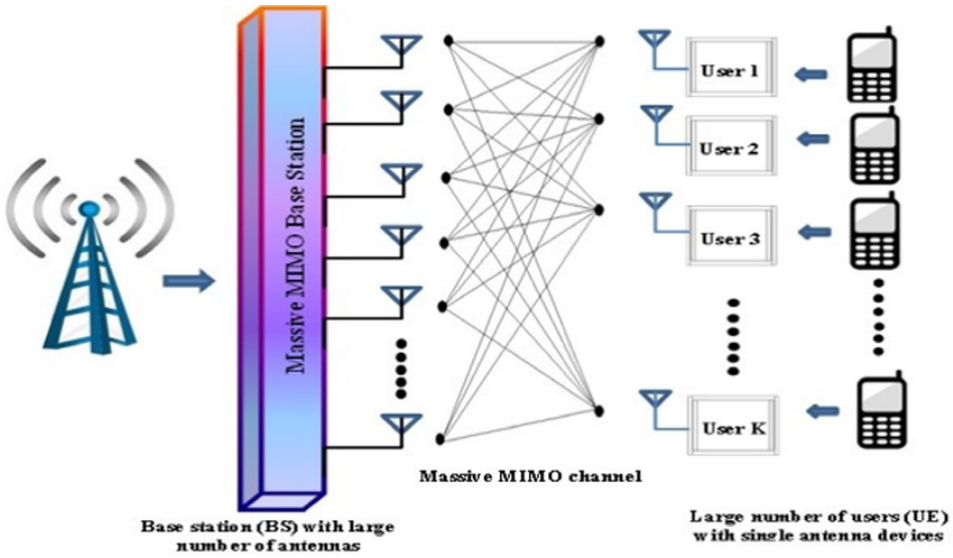

Figure 1.8: Massive-MIMO basic architecture

1.2.3 The sixth generation (6G)

Sixth generation (**6G**) mobile networks are being developed and are expected to offer unrestricted wireless communication. This technology aspires to achieve terabit-level transmission speeds. To support 6G technology, smart antennas, more memory in mobile devices, and wide-area optical networks will be required. Unlike previous generations, 6G networks will be cell-free, and will enable the integration of artificial intelligence into wireless networks. While the specific frequency bands for 6G have not yet been determined, it is clear that a much higher frequency band is needed to increase the data rate required for 6G networks [1]. While 6G is associated with much higher frequency in the terahertz range ($300GHz$ to $3terahertz$). 6G networks are expected to be introduced in 2030 [17]. The advantages of 6G networks include:

- **Data rate:** 6G networks provide a much higher data rate, up to 1$terabytespersecond$. It facilitates the transfer of massive amounts of data faster and more efficiently, which is about a hundred times better than 5G networks.
- **Latency:** Low latency of 0.1$milliseconds$ compared to 1$millisecond$ provided by 5G networks.
- **Energy efficiency:** 6G networks provide more efficient use of energy and increase the efficiency of their network by 100 times compared to 5G networks.
- **Broadband connectivity:** Massive broadcast data, which can support more than a million connections, which is about a hundred times more than 5G networks.
- **Increased capacity:** 6G networks have a capacity of up to $1,000$ times that of 5G networks.
- **Enhanced reliability :** 6G networks are superior to 5G networks in terms of reliability. Therefore, new technologies such as quantum communications and terahertz (THz) waves will be used [18].

1.2.3.1 Tera Hertz Wave (THz)

In order to meet key performance indicators like peak rates of $1Tb/s$, extremely ultra-reliable low-latency communications, and high energy efficiencies of $1Tb/J$, THz will play a particularly significant role in 6G networks. It is anticipated that THz communications will enable real-life solutions and services in coexistence with the heavily saturated sub-$6GHz$ and millimeter-wave spectra [19] .

Terahertz waves are electromagnetic waves that have wavelengths between $30\mu m$ and $3mm$, vibration cycles between $0.1ps$ and $10ps$, and frequency between $0.1THz$ and $10THz$. Consequently, terahertz waves are classified as sub millimeters that fall between millimeter waves and infrared light in the field of optics, and they are part of the far-infrared spectrum in radio physics. as shown in Figure 1.9. Because of its unique physical characteristics, terahertz waves have found extensive usage in a variety of industries, including communications, aerospace, and medicine [20].

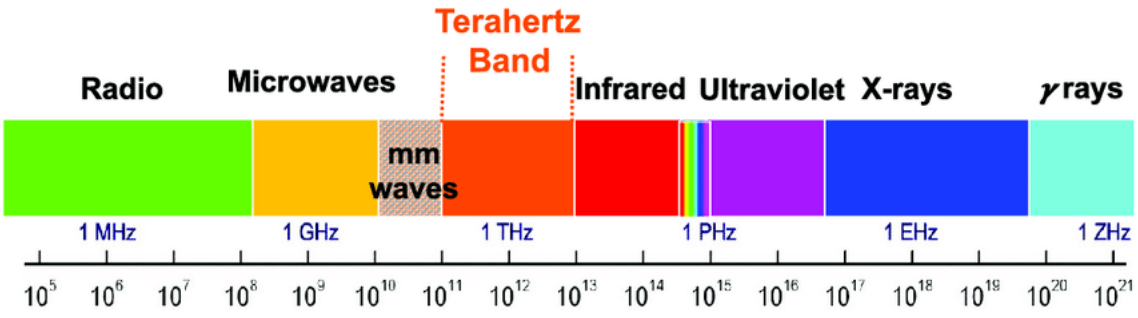

Figure 1.9: Schematic Diagram of Terahertz Wave Frequency Band

The frequency range:

The frequency range between 0.1 and 10$terahertz(THz)$, which is between the millimetre waves and infrared portions of the electromagnetic spectrum, is known as the terahertz band. Because of its small wavelengths, it is often referred to as submillimeter radiation. The sub-terahertz range (0.1 to 0.3THz) and the principal terahertz range (0.3 to 10THz) are the two primary sub-ranges into which this band is usually separated. In terms of spectrum, the band between 0.3 and 3THz is classified as far-infrared, whereas the portion between 275 and 300GHz is regarded as belonging to the millimetre wave spectrum. Given its capacity to handle extraordinarily high data rates, the terahertz band is a promising option for next-generation communication technologies, including 6G networks [21].

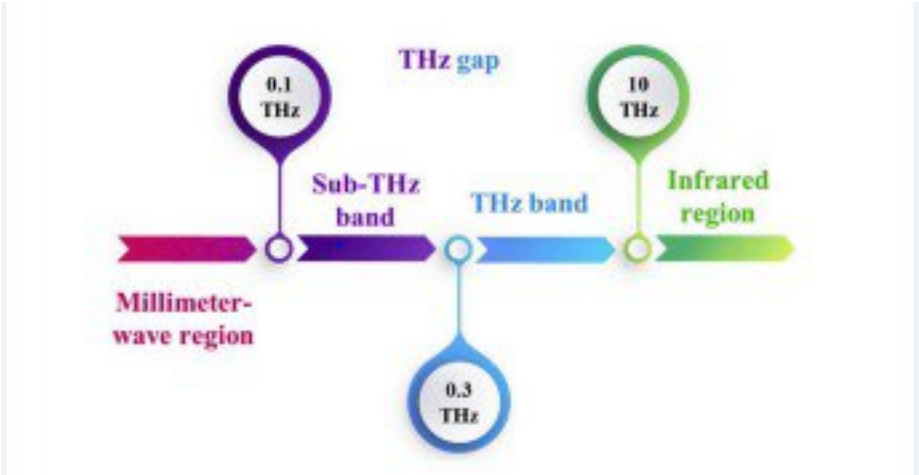

Figure 1.10: Frequency range in 6G wireless communication system

1.2.3.2 Ultra in 6G technology

Ultra-massive MIMO, a variant of LTE Evolution (Long-range MIMO) and Massive MIMO, uses hundreds or thousands of antenna elements at a base station to serve

dozens or hundreds of users simultaneously. Ultra-massive MIMO is the ideal choice for realizing the promise of 6G. It has the potential to significantly improve spectrum efficiency, power efficiency, and channel capacity [22]. The main functions and benefits of ultra-massive MIMO in 6G are:

1. **Larger capacity:** Ultra-massive MIMO uses massive arrays at both the transmitter and receiver ends to achieve spatially selective beamforming.
2. **Increased spectrum efficiency:** Ultra-massive MIMO enables the simultaneous transmission of multiple data streams due to its multiple antennas.
3. **Interference management:** Ultra-massive MIMO technologies can reduce interference from nearby cells or users.
4. **Extended Coverage:** Ultra MIMO technology can increase the coverage area of the base station by adding more antennas. This increases signal reception in hard-to-reach areas [23].

1.3 Challenges of Massive MIMO

Massive MIMO technology is more than just an expansion of MIMO technology, and there are still a lot of problems and obstacles to overcome before it can be used. The following lists some of the main difficulties with huge MIMO systems [24].

1.3.1 Signal detection

Signal detection is the process of identifying, extracting, and recovering the transmitted data sent by the user equipment (UE) over a communication channel from the signal received at the base station (BS), where all the signals sent by the users at the base station accumulate to create interference, which also contributes to the reduction of throughput and spectral efficiency. The main goal is to reduce the effect of noise and interference and recover the original symbols with the highest possible accuracy [25].

The uplink channel is used to transmit data and the pilot signal from the user terminal to the base station, as shown in Figure 1.11.

In the uplink channel of an mMIMO system, we consider a base station with M antennas serving K users of a single antenna at the same time, such that $M >> K$. The symbol vector $s = [s_1, s_2, \cdots, s_K]^T \in \mathbb{C}^{K\times 1}$ denotes the signal transmitted by all users, and the symbol vector $y = [y_1, y_2, \cdots, y_M]^T \in \mathbb{C}^{M\times 1}$ denotes the signal received at the base station. The channel between K users and M antennas of the base station forms a channel matrix $H \in \mathbb{C}^{M\times K}$ defined by a set of flat Rayleigh complex vanishing coefficients, whose

elements are independent and identically distributed (i.i.d.), generated by Gaussian random variables with zero mean and unit variance σ^2 [26].The relationship between s, y and H can be modeled as:

$$y = H_s + n, \tag{1.1}$$

where: n: Is the Gaussian white noise following a Gaussian distribution, and the mathematical expectation is 0. The variance is σ^2, H: Channel matrix.

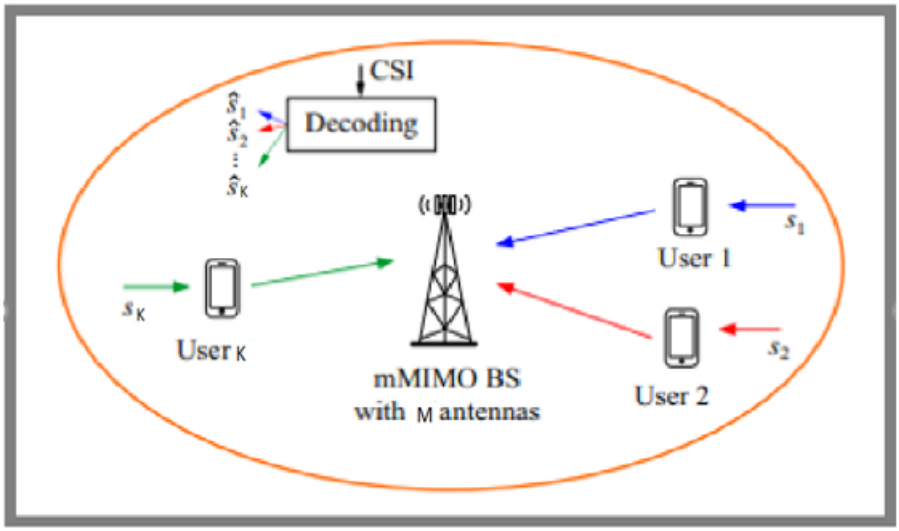

Figure 1.11: Uplink massive MIMO system model with M antennas BS serving K user

Massive MIMO systems' many antennas make UL uplink signal recognition computationally challenging, which lowers possible throughput. Both conventional and contemporary methods, such as successful interference cancellation (SIC) and spherical decoder (SD), are used to obtain good performance. Matching filter (MF), zero-force (ZF), and mean least square error (MMSE) are examples of low-complexity linear signal detectors that are advised for use in massive MIMO systems [23].

1.3.2 Precoding

Precoding is a transmitter signal processing technique required to maximize the received signal for certain receivers and other antennas. In massive MIMO systems, precoding is an effective approach that enhances throughput while minimizing the effects of path loss and interference. The UL pilot signals transmitted from the receiving stations allow the base station (BS) to estimate the CSI. However, due to various environmental obstructions on the channel, the CSI received at the BS is imperfect and uncontrolled.

In massive MIMO, the base station uses precoding strategies based on the available CSI. Despite the advantages offered by massive MIMO, it suffers from high computational complexity due to the large number of antennas. Therefore, low-complexity techniques and processors are necessary for massive MIMO systems [27].

In a downlink massive MIMO system, the base station is equipped with M antennas serving K users with one antenna at the same time, where $M \geq K$. In TDD mode, the transport channel in DL is the transport channel of the transport channel matrix in UL due to the reciprocity of the channel. The vector $a = [a_1, a_2, \ldots, a_K]^T$ indicates the received data, which are taken from an Mary constellation, went through a precoding stage at the BS for the DL transmission. By transforming a into an $M \times 1$ vector as $x = [x_1, \ldots, x_M]^T$, the M BS antennas create their precoded vector, which they then deliver independently to each terminal of the K-received terminals over the channel. The precoder can be used to direct the broadcast signal to the designated received terminal, provided that the BS is synchronized and the CSI is flawless. Massive MIMO systems with M-transmitted antennas and K-received terminals are depicted in Figure 1.12, which also displays the precoding block's location. $y = [y_1, y_2, \ldots, y_K]^T$ is the received vector, which is affected by noise and channel effects. At the base station, the $K \times 1$ vector of the received signal can be expressed as [27].

$$y = H^T x + n \quad \text{where } y \in \mathbb{C}^{k \times 1}, \tag{1.2}$$

The channel matrix $H \in \mathbb{C}^{M \times k}$. can be represented as

$$H = \begin{bmatrix} h_{11} & \cdots & h_{1k} \\ \vdots & \ddots & \vdots \\ h_{M1} & \cdots & h_{Mk} \end{bmatrix}, \quad H \in \mathbb{C}^{M \times K},$$

where n is an $K \times 1$ additive white Gaussian noise (AWGN) vector whose elements are drawn from complex Gaussian distributions $CN(0, \sigma^2 n)$
In the DL transmission, where $M > K$, the transmitted signal for the K users can be written as follows:

$$x = \sqrt{\rho} P a, \text{ where } x \in \mathbb{C}^{M \times 1}, \tag{1.3}$$

where $\sqrt{\rho}$ is the transmitted average power, a is an $K \times 1$ transmitted vector prior to the precoding operation, and P is an $M \times K$ linear precoding matrix. H is connected to the precoding matrix P. The DL channel is the transpose of the H in the TDD mode, and

the $K \times 1$ vector at K-received terminals becomes [27].

$$y = H^T x + n \tag{1.4}$$

$$\sqrt{\rho} H^T P a + n, \quad y \in \mathbb{C}^{k \times 1}. \tag{1.5}$$

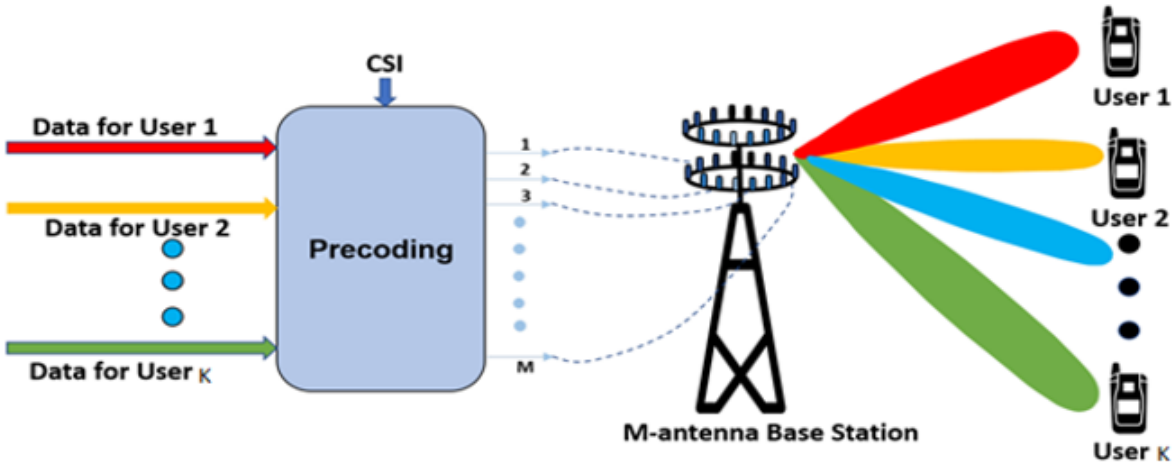

Figure 1.12: Precoding in a massive MIMO

Precoding methods come in two types: linear and nonlinear. ZF and MMSE are examples of linear precoding systems that work by multiplying the transmitted signal by a precoding matrix. They work well as a non-discontinuous system. However, generating a quasi-inverse matrix is computationally difficult. Nonlinear precoding methods, such as directional perturbation (VP) and dirty paper coding (DPC), are theoretically efficient and work well, but are complicated by their infinite length requirements [22].

In 6G, new pre-modulation techniques using artificial intelligence and deep learning are also used for providing higher accuracy (AL/ML), and yet another new innovation to improve the performance of the wireless network indoors and outdoors is the intelligent reconfigurable surface (IRS/RIS) technology, which is changing signal parameters with low-cost passive devices [28].

1.3.3 Channel estimation

Channel state information (CSI) is used by massive MIMO systems for signal detection and decoding. Through the use of channel estimating techniques, the

combined impacts of path loss, delay propagation, fading, dispersion, and other channel characteristics are represented by CSI. The present status of the communication link between the transmitter and the receiver is ascertained using this information [24]. FDD and TDD wireless modes are depicted in Figure1.13a, while a typical empirical transmission mechanism and **CSI** feedback system in FDD and TDD modes are shown in Figure1.13b [1].

Recent years have seen the development of numerous techniques for channel estimation in massive MIMO systems that combine low computational cost and good spectral efficiency. Blind estimation, semi-blind estimation, and heuristic-based estimation are the three most popular estimation techniques.

Although the reference presents low-complexity least squares (LS) estimation, its accuracy is not optimal. To attain energy efficiency, a linear minimal mean square error (MMSE) technique has been suggested. It depends on sending reference symbols that have already been established. Despite offering the best accuracy, MMSE becomes more computationally complex as the number of antennas increases. The literature, on the other hand, suggests a blind channel estimation technique that depends on the received signal's subspace properties. To enhance downlink channel estimates, machine learning (ML) in conjunction with compressed sensing (CS)-based channel estimation has been suggested in the literature. To get more precise channel estimations, semi-blind channel estimating techniques combine the two previously discussed approaches. These techniques are crucial for 6G systems in order to improve accuracy since they offer accurate beam steering, reduce computational complexity, and preserve high estimation accuracy [23].

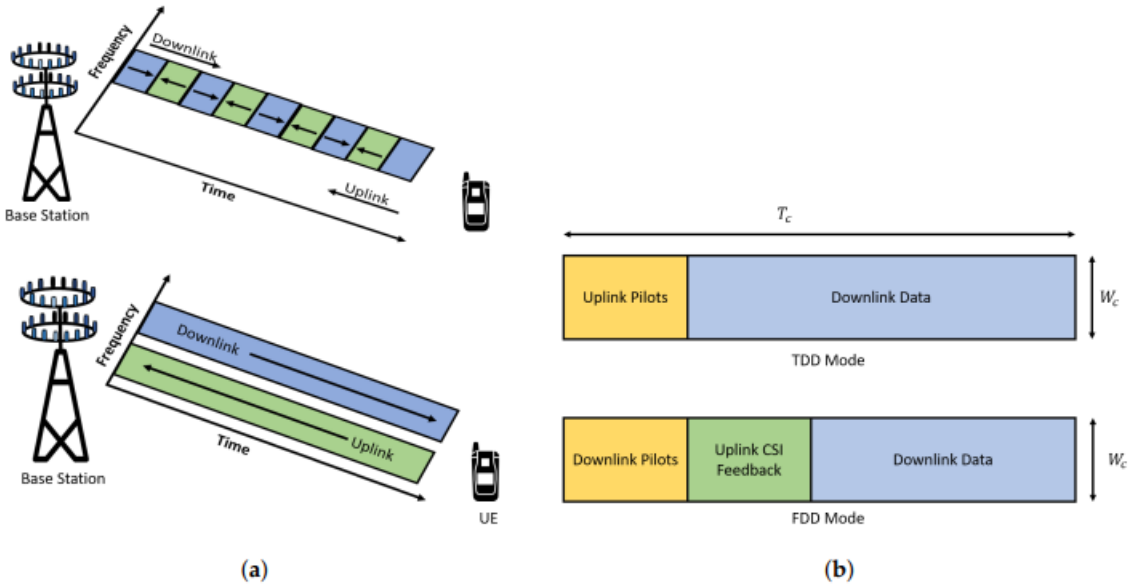

Figure 1.13:
(a): Frequency Division Duplexing (FDD) and Time Division Duplexing (TDD) mode: Massive works best in TDD mode.
(b): Typical pilot transmission and CSI feed back mechanism in FDD and TDD mode.

Least Squares Channel Estimation

An essential method for estimating the channel state information (CSI) between the transmitter and receiver in wireless communication systems is the least squares (LS) method. Using this method, known signals are sent and received, and the difference between the sent and received signals is then calculated [29]. The following is the estimation formula:

$$y = Hx + n, \tag{1.6}$$

The estimate of H is obtained by solving the least squares problem as follows:

$$\widehat{H} = \|Hx - argmin_H\|^2 y, \tag{1.7}$$

where: y: is the vector of the received signal, H: is the channel matrix to be estimated, x: is the transmitted (training) signal vector, n: is the noise vector. To find H, we solve for the zeroth derivative of the equation with respect to H. This gives us the following closed form solution:

$$\widehat{H}_{LS} = (X^H X)^{-1} X^H Y. \tag{1.8}$$

1.4 Comparison between 4G and 5G and 6G Technology

Features	4G	5G	**6G**
Pack data rates	DL to $1Gb/s$	DL to $20Gb/s$	DL to $100Tb/s$
	UL to $100Mb/s$	UL to $10Gb/s$	UL to 1Tb/s
Frequency band	Sub $6GHz$ (1 to 6 GHZ)	Sub 6GHz & mmwave (30 to $300GHz$ / $24-100GHZ$)	Sub $6GHz$ mmwave band + Terahertz band ($0.1THz$ to $10THz$)
Number of Antennas MIMO	MIMO 2×2 4×4 8×8	Massive MIMO (64×64 to 256×256)	Ultra-massive MIMO 1024×1024
Latency (ms)	$50ms$	$1ms$	$0.1ms$
Traffic Capacity	$10Mb/sm^2$	$100Mb/sm^2$	1 to $10Gb/sm^2$

Localization precision	5 to 10 meters	10cm in 2D	1cm in 3D
Use Cases	Mobile broadband, video streaming, basic IoT	Enhanced mobile broadband, IoT, AR/VR, smart cities, connected vehicles	Advanced IoT applications, AI-driven services, immersive AR/VR, holographic communication
Mobility support	UP to 350Km/h	UP to 500Km/h	UP to 1000Km/h
Maximun spectral efficiency	15$bits/Hz$	30$bits/Hz$	100$bits/Hz$
Technology	LTE, OFDMA, MIMO	Massive MIMO, mmWave, Beamforming	AI, THz, RIS, Holographic MIMO

Table 1.1: Showing the comparison between 4G, 5G and 6G technology

1.5 Conclusion

Our analysis of this chapter led to the conclusion that, while the fourth generation still provides high-speed connectivity, the fifth generation (5G) has introduced advanced technologies such as massive MIMO, packet formation, and millimeter waves. These innovations have resulted in reduced latency, improved spectral efficiency, and significantly higher data speeds. In contrast, the sixth generation (6G) leverages terahertz waves and ultra-massive MIMO technology to achieve transmission times as low as 0.1 milliseconds and data speeds reaching up to terabytes per second. Ultimately, we conclude that each generation of wireless communication offers enhanced capabilities and higher speeds than the previous one.

Chapter 2

Role of Intelligent Reflective Surfaces (IRS) in Improving Wireless Network Performance

2.1 Introduction

In this chapter, we explore advanced telecommunications network technologies, including the emergence of intelligent reflective surfaces (IRS), a new technology designed to improve signal quality and efficiency and enhance coverage in hard-to-reach areas. This chapter also includes an examination of the concept of this technology and how its architecture is formed, as well as an introduction to its types, including passive and active. It also covers its applications in various fields and its uses for improving coverage. We compare IRS technology to relays and massive MIMO, discuss the use of massive MIMO systems, relaying, and IRS-enabled systems, and address the impact of path loss. Finally, we examine the challenges affecting the operation of the IRS and explore the strategies used to address these problems.

2.2 Intelligent reflecting surfaces

An IRS system consists of a flat surface containing multiple small, inexpensive, and independently reconfigurable passive reflective elements to alter the phase of the reflected signal. IRS systems can be classified into two types: antenna array-based systems or reflective surface-based systems. The reflected signals can be reconfigured to propagate in the desired directions by precisely changing the phase shifts of each reflective element [30]. Additional names for this type include large smart surfaces (LIS), which describe surfaces that bypass massive multiple-input/output (MIMO) technology, and digital steerable hubs (DCS), highlighting their ability to digitally control devices covered with smart surfaces [31].

A typical IRS system consists of three main layers: The outer layer consists of various reflective components printed on an insulating layer, directly affecting the incoming signals. The middle layer features a copper foil, which prevents power and signal leakage during reflection. The inner layer is a circuit board controlled by a smart device, such as an FPGA, which adjusts the reflection parameters of the IRS elements, as shown in Figure 2.1.

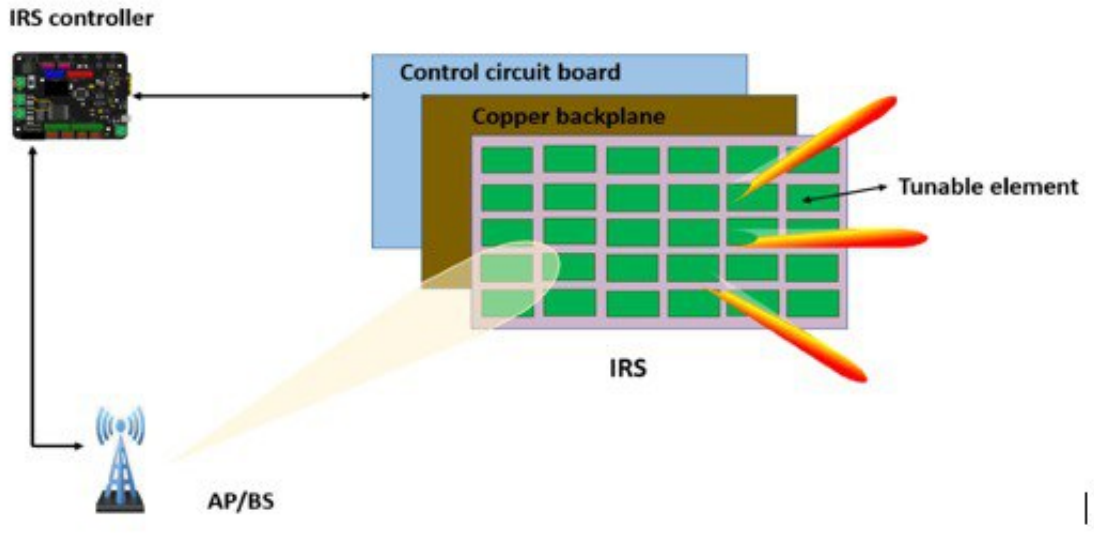

Figure 2.1: Architecture of an IRS Structure Layers.

The ideal reflection coefficients for the IRS are determined at the base station and sent to the IRS controller via a dedicated feedback link in a typical operating scenario. Channel State Information (CSI), which is updated only when changes occur, is used to determine the reflection coefficients, and the time required is much longer than the length of the data symbols. Each reflecting element contains PIN diodes, as shown in Figure 2.2(a). As illustrated in the corresponding circuit shown in Figure 2.2(b), these diodes switch between ”on” and ”off” by adjusting the voltage [30].

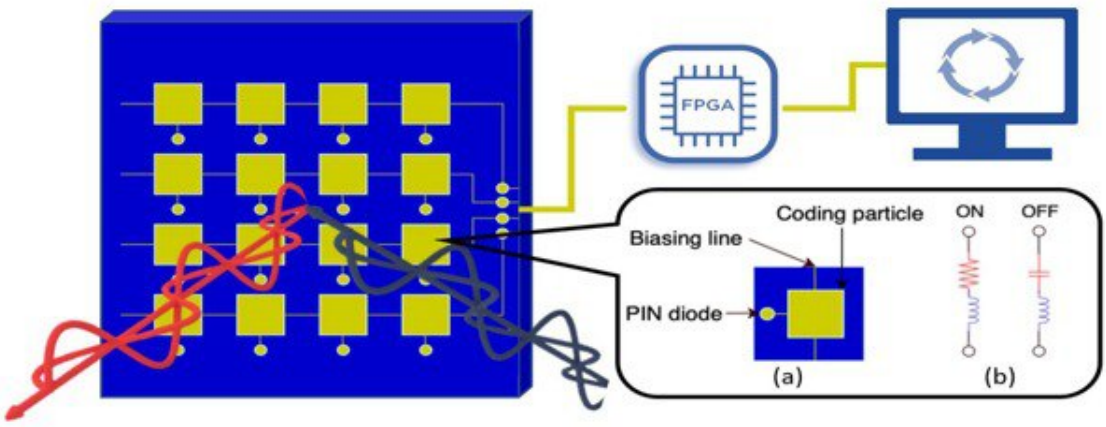

Figure 2.2: Architecture of an IRS.

2.3 Passive IRS and Active IRS

There are two types of IRSs: passive and active. Passive smart surfaces only use their reflective qualities to reflect signals, they don't amplify them. On the other hand, active smart surfaces possess amplifiers that enable them to enhance reflected signals.

2.3.1 Passive IRS

An IRS, another name for a passive radio frequency (RF) reflector, is made up of several passive reflective components with positive resistances. It does not require signal processing or amplification in order to reflect the incoming signal with a phase shift. This system is immune to self-interference and runs in full-duplex mode. The reflected signal can be merged either destructively to lessen undesired interference or constructively to increase signal strength. As seen in Figure 2.3.a, this is accomplished by suitably modifying the phase shifts of each passive reflective element. However, the length of the reflected path causes signal loss, which is a concern for the system. By putting the IRS closer to the transmitter and/or receiver or adding more reflective features, this can be avoided [32].

2.3.2 Active IRS

Each active reflector element in an active IRS system contains an active load (negative resistance), such as a negative-impedance transformer or tunnel diode. To amplify the signal, each load is connected to a separate power supply, as shown in Figure 2.3 b. As a result, an IRS system allows for amplification of the incoming signals in full-duplex mode, as well as phase control, but at a slightly higher hardware and power cost compared to passive systems. It also has advantages over passive systems. Active IRS systems use active components to amplify the low thermal noise introduced by passive IRS systems. However, they can still achieve a better signal-to-noise ratio because beamforming allows the receiver to coherently combine the necessary signals from multiple active IRS elements in the same phase [32].

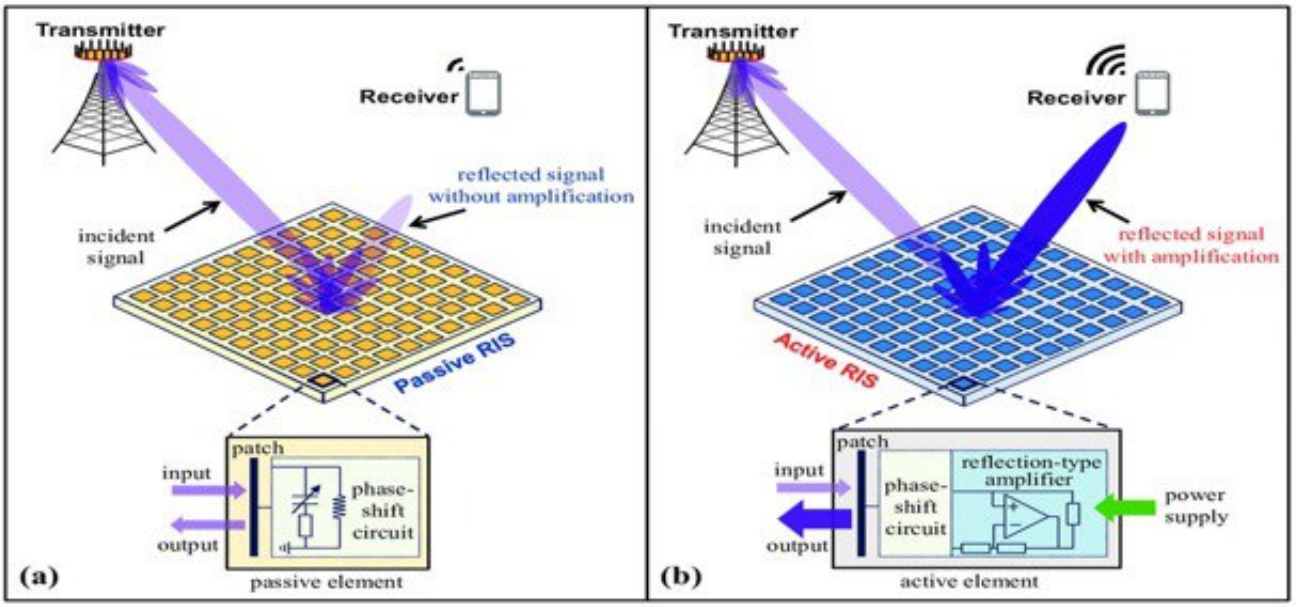

Figure 2.3: An illustration of the hardware architectures of (a) a passive IRS and (b) an active IRS.

2.4 The IRS applications

Reflected signals can be combined either destructively or constructively to enhance the strength of the desired signal by carefully adjusting the phase shifts of the IRS reflector elements. IRS systems provide greater flexibility, significantly improving overall system performance and signal enhancement.Figure 2.4 displays various typical uses of IRS-enabled wireless networks [30].

- The first application examines a scenario where a user is located in an isolated area, facing significant communication challenges due to an obstacle that obstructs direct contact with the base station. In this case, intelligent signal reflection from an IRS can help circumvent the obstacle, effectively creating a virtual line of sight (LOS) between the user and the base station.

- The second application demonstrates the use of an IRS system to enhance physical layer security. Possible communication confidentiality rates are severely limited when the eavesdropper is in the same direction as the legitimate user (such as User 2) or when the link distance between the base station and the eavesdropper is less than the distance to the legitimate user (such as User 1). In this case, by placing the IRS system close to the eavesdropper, the reflected IRS signal can be modulated to block the base station signal (not reflected from the IRS system),

effectively reducing information loss [33].

- In a third application, an IRS system can be installed at the cell edge to improve the desired signal strength and suppress interference through a suitable reflection beam design. This creates a ”signal hotspot” and an ”interference-free zone” around the cell edge for a user experiencing high signal attenuation and severe channel interference [33].
- The fourth application focuses on device-to-device (D2D) networks, where IRS can be used to optimize individual data links in these communication systems, support the low-power transmission required in these systems, and eliminate interference [33].
- The fifth application is the use of IRS systems in the millimeter wave band, where propagation is highly sensitive to obstructions. In these cases, IRS systems help increase the spatial diversity required for outdoor systems by increasing the received power and channel arrangement.
- The sixth application is the use of IRS in Internet of Things (IoT) systems. In power-constrained IoT networks, the multi-IRS scenario appears to be useful in compensating for power loss over long distances and solving the power budget problem through passive IRS beamforming [33].
- The seventh application represents a promising multiple access strategy using NOMA. This strategy significantly improves the spectrum efficiency of conventional orthogonal multiple access (OMA). However, NOMA may not be effective when user channel vectors are orthogonal. Here, an IRS system can be incorporated to reshape wireless channel vectors, allowing for their convergence and extending the scope of NOMA use [30].

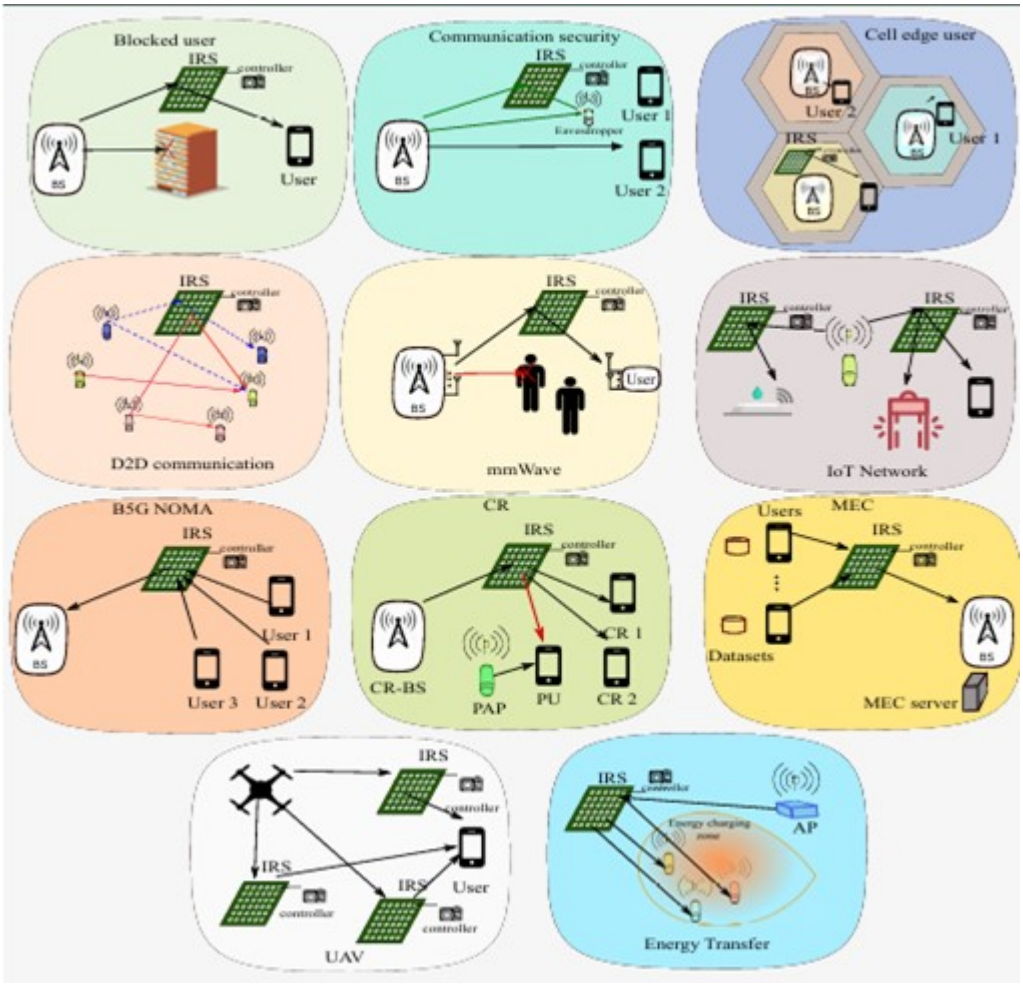

Figure 2.4: Typical applications of IRS in various emerging Sub-6 GHz systems.

2.5 Comparison of IRS Systems with Other Related Technologies

IRS provides a completely new solution and, thus, a competitive advantage when compared to other closely related technologies that are being utilized in non-wireless networks, such as MIMO, AF, and Decode and Forward (DF) [34].

2.5.1 The difference between IRS and Massive MIMO:

Both massive MIMO and IRS systems use large-scale arrays to achieve significant improvements in beamforming, but there are three key differences between them:

First, an IRS system consists of passive components such as capacitance and inductance and is incapable of processing data, while a Massive MIMO system uses active components (RF circuits and signal processing units). This difference accounts for the lower cost and power consumption of a IRS system. Second, IRS systems

passively reflect incoming signals, while a massive MIMO system generates, transmits, or receives signals .Finally, the distance between IRS elements is much less than half a wavelength, unlike the half-wavelength spacing of antennas in massive MIMO systems. This is because IRS systems only reflect [35].

2.5.2 The difference between IRS and relay:

Since both IRSs and current relays can serve as aids to improve wireless communications between the transmitter and the receiver, they are also seen to be comparable. But there are a number of significant distinctions [35].

- **IRS vs. AF Relay:** An IRS eliminates the need for transmit power consumption by reflecting incident signals as a passive array without a transmitter, whereas AF relays aid in source-destination transmission by regenerating and boosting the signals. An IRS is designed to function in full duplex mode, which makes it more spectrum efficient, whereas AF operates in half duplex mode due to heavy interference in full duplex mode, which requires effective interference cancellation techniques [34].
- **IRS vs. DF Relay:** DF relays work similarly to AF relays in that they decode and retransmit the signal from the source to the destination. They are substantially more complicated and require a lot of signal processing power because of the decoding process. IRS systems, on the other hand, just engage in passive reflection and do not decode, as was previously mentioned. As a result, they are less costly and use less electricity [34].

2.6 Path Loss

By creating a path loss model to examine the received signal strength and SNR performance, it is possible to confirm the possible performance boost of implementing IRS in wireless networks. Each IRS's reflecting element offers a second path from the transmitter to the receiver in addition to the direct path, as seen in Figure 2.5, creating a two-way signal propagation model. The received signal power can be obtained as follows by combining the signals from all paths:

$$P_r = P_t \left(\frac{\lambda}{4\pi}\right)^2 \left|\frac{1}{\ell} + \sum_{n=1}^{N} \frac{R_n e^{-j\Delta\Phi_n}}{d_{1,n} + d_{2,n}}\right|^2, \tag{2.1}$$

where N is the number of IRS-reflecting elements and ℓ is the direct path distance,

which can be approximated by the distance between the transceivers. The symbols $d_{(1,n)}$ and $d_{(2,n)}$ indicate the separations of two segments in the reflected path via the nth reflecting element. The summing term (2.1) indicates the signal reflection across several paths. The phase difference is determined by the distances of the direct path and the reflected path via the nth reflecting element. The reflection coefficient, denoted by R_n, is dependent on the electromagnetic properties of the reflecting object and is frequently unmanageable without the application of IRS.

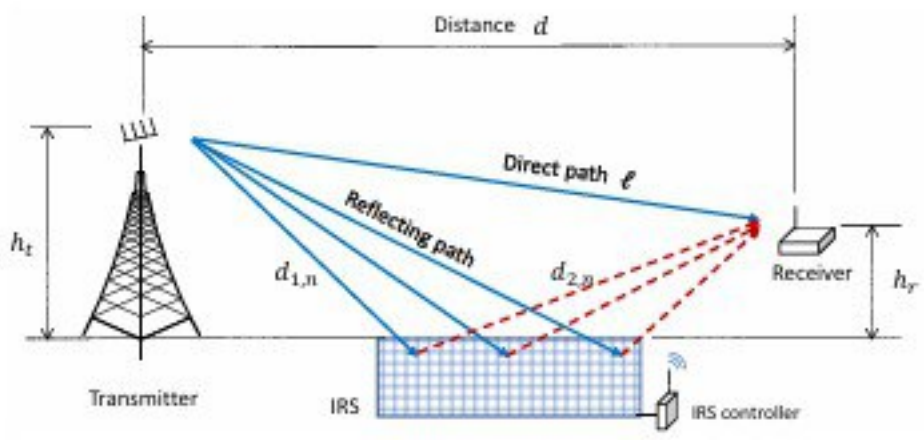

Figure 2.5: Two-way channel model for IRS-assisted wireless communications.

The reflected signal can be coherently aligned with the direct path by proactively controlling the phase shift of each reflecting element on the Intelligent Reflecting Surface (IRS). This is represented as $R_n = e^{-j\Delta\Phi_n}$. Typically, we can assume that d approx. $d \approx \ell = d_{1,n} + d_{2,n}$, which leads to the approximation of the received signal power as described in equation (2.1).

$$P_r \propto (N+1)^2 P_t \left(\frac{\lambda}{4\pi d}\right)^2, \tag{2.2}$$

If the size N of reflecting elements increases or there is no direct link, the path loss mentioned above can be easily recast as $P_r \approx N^2 P_t \left(\frac{\lambda}{4\pi d}\right)^2$. In contrast to the free-space path loss model, the IRS-assisted path loss in (2.2) increases the received signal power by a certain amount so that the received power is proportional to N^2.

The compound channel from the transmitter to the receiver can be thought of as a Gaussian-distributed random variable with the mean and variance proportional to N for a large number of scattering elements with optimal phase configuration. This suggests that the average received SNR will rise proportionately to N^2.

Basic knowledge of IRS superiority in wireless communications is fostered by the simplified path loss model in (2.2), but it leaves out intricate physical details of IRS-assisted signal propagation, such as the size and dimensions of the reflecting elements, the angles of incident and reflected signals, and the anisotropic radiation pattern of the antennas at the transceivers.

Considering the transmit power and transceiver sites, the ideal received signal power in the far field can be described as follows:

$$P_r \propto G_C N^2 P_t \left(\frac{\lambda}{4\pi d_1 d_2}\right)^2 \left(\frac{\rho^2 F(\theta_t, \Phi_t) F(\theta_r, \Phi_r)}{4\pi}\right), \tag{2.3}$$

where d_1 and d_2 denote the distance from the transmitter to the center of the IRS and from the center of the receiver to the center of the receiver, respectively. The function $F(.,.)$ determines the power radiation pattern of the antennas at the transceivers. Specifically, $F(\theta_t, \Phi_t)$ returns the uniform power level when the elevation and azimuth angles of the transmitter are given by (θ_t, Φ_t), relative to the center of the transmitter. The constant P indicates that all reflecting elements use the same magnitude of reflection coefficients. The parameter G_C depends on the antenna gains at the transceivers, the unit dimensions, and the power radiation pattern. Reflecting element. Similar to (2.2), the path loss model in (2.3) implies that in both cases the received signal power is proportional to N^2 [36].

2.7 Channel estimation

In wireless communication systems, channel estimation is a fundamental process that enables a precise understanding of the wireless channel parameters between the transmitter and the receiver. The passive nature of Reconfigurable Intelligent Surface (RIS) elements, combined with the complex, high-dimensional channels they create, makes channel estimation significantly more challenging in RIS-assisted systems.

Unlike traditional relays, RIS-assisted systems consist of passive components that lack active RF chains. This limitation creates a major bottleneck in acquiring CSI, as these passive components cannot directly transmit, receive, or process pilot signals [37].

2.7.1 Cascaded Channel

We keep all components of the RIS activated, as illustrated in Figure 2.6. The RIS and base station (BS) each have N elements and M antennas, set up in a uniform planar array (UPA) layout to support K users with single antennas simultaneously. The channel

betwene RIS and the BS are represented G as $\mathbb{C}^{N\times M}$, while the channel from the kth user to the RIS is denoted by $h_{r,k} \in \mathbb{C}^{N\times 1}$ (where $k = 1, 2, \ldots, K$). We utilize the Saleh-Valenzuela channel model to characterize the channel between the RIS and the BS, as detailed below:

$$G = \sqrt{\frac{NM}{L_G}} \sum_{\ell_1=1}^{L_G} \alpha_{\ell_1}^{G} b(v_{\ell_1}^{Gr}, \Psi_{\ell_1}^{Gr}) a(v_{\ell_1}^{Gt}, \Psi_{\ell_1}^{Gt}) \tag{2.4}$$

Where L_G is the number of paths connecting the RIS and BS, and $\alpha_{\ell_1}^{G}$, $v_{\ell_1}^{Gr}(\Psi_{\ell_1}^{Gr})$, $v_{\ell_1}^{Gt}(\Psi_{\ell_1}^{Gt})$ is the complex gain, the azimuth (elevation) angle at the BS and RIS for the ℓ_1 path, respectively. Similarly, the UE-RIS channel can be represented by

$$h_{r,k} = \sqrt{\frac{N}{L_{r,k}}} \sum_{\ell_2=1}^{L_{r,k}} \alpha_{\ell_2}^{r,k}\, a(v_{\ell_2}^{r,k}, \Psi_{\ell_2}^{r,k}) \tag{2.5}$$

Where $L_{r,k}$ is the number of paths between the kth user and RIS, $\alpha_{\ell_2}^{r,k}$, $v_{\ell_2}^{r,k}(\Psi_{\ell_2}^{r,k})$ is the complex gain, and the azimuth (elevation) angle at the RIS for the ℓ_2 path, respectively. A $(v, \Psi) \in \mathbb{C}^{N\times 1}$ represents the steering vector for the normalized array at the RIS.

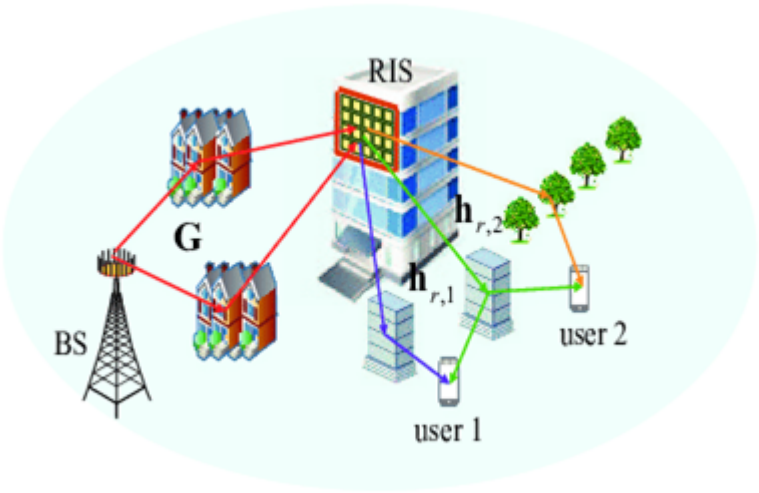

Figure 2.6: Channel Structure in IRS-Aided MIMO System.

$H_k = G\,diag(h_{k,r})$ is the definition of the kth user's $N \times M$ cascaded channel, which we then translate to an angular domain representation as

$$H_k = U_M \widehat{H}_k U_N^T \tag{2.6}$$

Where $\widehat{H}_k$ is the $N \times M$ angle cascaded channel, and U_M and U_N are the BS's and RIS's respective $M \times M$ and $N \times N$ dictionary unitary matrices.

Using an orthogonal pilot transmission technique to estimate the uplink channel, all users send known pilot symbols to BS via RIS in Q time intervals. Once the direct channel impact between the BS and UE has been eliminated, the effective received signal for the kth user at the BS in the qth $(q = 1, 2, \dots, Q)$ time slot can be written as $y_{k,q} \in \mathbb{C}^{M\times 1}$

$$y_{k,q} = H_k \theta_q x_{k,q} + n_{k,q} \tag{2.7}$$

where $x_{k,q}$ is the pilot symbol that the kth user sends, $\theta_q = [\theta_{q,1}, \theta_{q,2}, \dots, \theta_{q,N}]^T$ is the reflecting vector of RIS, the reflecting coefficient at the nth RIS element $(n = 1, 2, \dots, N)$ in the qth time slot is given by $\theta_{q,n}$, and $n_{k,q} \sim CN(0, \sigma^2 I_M)$ is the $M \times 1$ received noise with σ^2 representing the noise power [38].

For Q time slots following pilot transmission, let $x_{k,q} = 1$, and we obtain the overall measurement matrix of $\mathrm{Y}_k = [y_{k,1}, y_{k,2}, \dots, y_{k,Q}]$.

$$\mathrm{Y}_k = H_k \Theta + N_k \tag{2.8}$$

where $\Theta = [\theta_1, \theta_2, \dots, \theta_Q]$, and $N_k = [n_{k,1}, n_{k,2}, \dots, n_{k,1}]$.

Compressed Sensing for Channel Estimation

Compressed Sensing (CS) techniques are employed to reduce the computational load and the number of pilot signals needed, as the channels of RIS in the angular domain are sparse.

The Orthogonal Matching Pursuit

In a compressed sensing environment, the Orthogonal Matching Pursuit (OMP) algorithm is an iterative method for reconstructing sparse signals from several linear measurements. The sensor matrix column (atoms) that has the strongest correlation with the current residual value is chosen by the OMP algorithm in each iteration. After combining the chosen columns to create a support set, a least-squares problem is solved on this set to update the signal estimate. Until a predetermined stopping criterion such as the maximum number of iterations or the residual energy threshold is satisfied, the process keeps going [39].

The Structured Sparsity Orthogonal Matching Pursuit

A multi-vector variation of the classic OMP algorithm, the sparse-structured orthogonal matching (SS-OMP) technique takes advantage of the shared variance among several measurement vectors. It works especially well when there is a common variance among

several signals. The algorithm chooses the sensor matrix column with the highest cumulative correlation among all residuals at each iteration [40].

The Double-Structured Orthogonal Matching Pursuit

A vector technique called DS-OMP (Double-Structured Orthogonal Matching Pursuit) is used in wireless communication systems to recover sparse signals. To increase estimation accuracy, it takes advantage of sparseness's dual structure, which includes angle and delay. By simultaneously calculating the fully shared non-zero rows and partially shared non-zero columns across all users, the algorithm chooses correlated blocks of components that are most closely related to the residual signal. The algorithm adjusts the support based on the block with the highest cumulative projection energy at each step. With fewer measurements and less processing complexity, this methodical technique increases the accuracy of the channel estimate [38].

2.8 Conclusion

In conclusion, we have highlighted the importance of IRS in enhancing wireless networks. By studying the fundamental principles and operational mechanisms of this technology, it has become clear that its integration can significantly improve communication quality and strengthen network performance. Additionally, we have identified solutions to the challenges of channel estimation through the application of a set of algorithms, which will be discussed in more detail in the application chapter.

Chapter 3

Performance Evaluation and Simulation of Intelligent Reflective Surface System

3.1 Introduction

The performance of wireless communication systems, including SISO, DF relays, and IRS, is thoroughly examined in this chapter. The impact of the number of IRS elements on signal amplification is examined by looking at channel models and analyzing energy efficiency, path loss, and channel gain. Using physical optics approaches, we also analyze the propagation model in IRS systems, considering the impact of reflection angles and surface size on path loss. Furthermore, channel estimation in RIS systems with huge MIMO antennas is examined using sophisticated algorithms to compare estimation performance under the effects of signal-to-noise ratio (SNR), distance, and the number of dispersants.

3.2 Analytical Performance Comparison Between SISO, IRS, and DF Relaying Systems

3.2.1 System Model and Channel Analysis

To evaluate system performance, we examine a communication configuration in which the variable d_1 determines the position of the destination, while the source and IRS/relay remain fixed. This configuration is illustrated in Figure 3.1, where the propagation characteristics are influenced by the distances between the various elements. We assume that both the source and the IRS/relay are equipped with antennas of specified gain, while the destination is a mobile device with an omnidirectional antenna. The channel gain is calculated based on these distances [41].

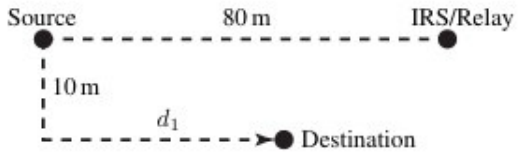

Figure 3.1: The simulation setup where d_1 is a variable

The IRS and relay are strategically positioned to establish LOS channels with the source, ensuring that direct signal propagation occurs. Therefore, we can express the total channel gain as $\beta_{IRS} = \beta_{sr}\beta_{rd}$, where β_{rd} indicates the channel gain between the IRS and the destination, and β_{sr} denotes the channel gain between the IRS and the source since the destination maintains a LOS link to the IRS/relay. However, if NLOS conditions arise, signal attenuation occurs on the direct link between the source and the

destination. This highlights the necessity of using an IRS or relays to compensate for the reduced channel gain and enhance transmission reliability.

3.2.2 Channel Gain

The channel gain is calculated using the following relationship:

$$\beta(d)[dB] = G_t + G_r + \begin{cases} -28 - 20\log_{10}(f_c) - 22\log_{10}(d) \\ -22.7 - 26\log_{10}(f_c) - 36.7\log_{10}(d) \end{cases} \tag{3.1}$$

where G_t is transmit antenna gain, G_r is receive antenna gain, f_c is carrier frequency, and d is distance between transmitter and receiver.

3.2.3 Channel Capacity of SISO, IRS, and DF Relaying

This SISO (single-input single-output) channel's capacity is:

$$R_{SISO} = \log_2\left(1 + \frac{p\beta_{sd}}{\sigma^2}\right) \tag{3.2}$$

The IRS-supported network's channel capacity is:

$$R_{IRS} = \log_2\left(1 + \frac{p(\sqrt{\beta_{sd}} + N\alpha\sqrt{\beta_{IRS}})^2}{\sigma^2}\right) \tag{3.3}$$

The maximum rate achievable with repetition-coded DF relaying is

$$R_{DF} = \frac{1}{2}\log_2\left(1 + \frac{2p\beta_{rd}\beta_{sr}}{(\beta_{sr} + \beta_{rd} - \beta sd)\sigma^2}\right) \tag{3.4}$$

p: is the transmit power.

α is the reflection amplitude coefficient.

σ^2 : is noise power.

3.2.4 Transmit Power Minimization Under Rate Constraints

The rate equations in (3.2)-(3.4)are used to determine the required transmit power for each of the three communication configurations, given that the destination demands a specific data rate R.

To achieve a data rate R in a SISO system, a specific amount of power is required

$$p_{SISO} = (2^{\overline{R}} - 1)\frac{\sigma^2}{\beta_{sd}} \tag{3.5}$$

The transmission supported by the IRS requires power. The transmission supported by the IRS requires power

$$p_{IRS} = (2^{\overline{R}} - 1)\frac{\sigma^2}{(\sqrt{\beta_{sd}} + N\alpha\sqrt{\beta_{IRS}})^2} \tag{3.6}$$

The transmission supported by the relay requires power.

$$p_{DF} = \begin{cases} (2^{2\overline{R}} - 1)\frac{\sigma^2}{\beta_{sd}} & \text{if} \quad \beta_{sd} > \beta_{sr} \\ (2^{2\overline{R}} - 1)\frac{(\beta_{sr}+\beta_{rd}-\beta_{sd})\sigma^2}{2\beta_{rd}\beta_{sr}} & \text{if} \quad \beta_{sd} \leq \beta_{sr} \end{cases} \tag{3.7}$$

Furthermore, for the IRS to outperform Decode-and-Forward (DF) relaying, the number of IRS elements must surpass a certain threshold, as indicated by the following equation:

$$N > \frac{\sqrt{\left(\sqrt{1 + \frac{2p\beta_{rd}\beta_{sr}}{(\beta_{sr}+\beta_{rd}-\beta_{sd})\sigma^2}} - 1\right)\frac{\sigma^2}{p}} - \sqrt{\beta_{sd}}}{\alpha\sqrt{\beta_{IRS}}}, \tag{3.8}$$

where p is transmit power, and α is amplitude reflection coefficient.

3.2.5 Total Power Minimization Under Rate Constraints

The total power consumption of the system, or P_{total} , encompasses both the transmit power and the dissipation of hardware components.

- **In the SISO case**

$$P_{total} = \frac{p_{SISO}}{V} + P_s + P_d \tag{3.9}$$

  where P_s and P_d represent the hardware-dissipated power at the source and destination, respectively, while $V \in [0, 1]$ indicates the efficiency of the power amplifier.

- **In the IRS case**

$$P_{total}^{IRS} = \frac{p_{IRS}}{V} + P_s + P_d + NP_e \tag{3.10}$$

  P_e represents the power dissipation per component, resulting from the circuitry needed for adaptive phase-shifting.

- **In the relaying case**, the source is active only half of the time

$$P_{total}^{DF} = \frac{p_{DF}}{V} + \frac{1}{2}P_s + P_d + P_r \tag{3.11}$$

where P_r represents the power dissipated by the hardware at the relay.

The received signal strength and the IRS's reflection efficiency are utilized to determine the optimal number of IRS elements, or N_{opt}. This ensures reliable communication quality while minimizing power consumption.

$$N_{opt} = \sqrt[3]{\frac{(2^{\overline{R}} - 1)\sigma^2}{\alpha^2 \beta_{IRS} P_e}} - \frac{1}{\alpha}\sqrt{\frac{\beta_{sd}}{\beta_{IRS}}} \tag{3.12}$$

3.2.6 Energy Efficiency

Energy efficiency refers to the ratio of the expected data rate to the total power used.

$$EE = \frac{B \times \overline{R}}{P_{total}}, \tag{3.13}$$

where B is the bandwidth, $(\overline{R})$ is the data rate, and P_{total} is the total power consumption.

3.3 Analyzing Path Loss in Intelligent Reflective Surfaces Through Physical Optics Methods

3.3.1 Preliminaries: passive metallic surface

When a plane wave strikes an ideal metal surface of finite size at a specific angle of incidence, θ, we examine how the electromagnetic field intensity reflected from the surface behaves. The following formula represents the strength of the reflected field at a distance [42]:

$$S(r, \theta_s) = \left(\frac{ab}{\lambda}\right)^2 \frac{Ei^2}{r^2} \cos^2(\theta_i) \left(\frac{\sin\left(\frac{\pi b}{\lambda}\left(\sin(\theta_s) - \sin(\theta_i)\right)\right)}{\frac{\pi b}{\lambda}(\sin(\theta_s) - \sin(\theta_i))} \right)^2, \tag{3.14}$$

where a and b are IRS the surface dimensions, λ is the wavelength, θ_i is the required angle of incidence, θ_s is the observation angle, and k_0 is the wave number.

3.3.2 System model for intelligent metasurfaces

To guide an incident wave toward a particular reflected direction, we examine the local surface phase distribution that an IRS needs to implement.

When Snell's generalized law is applied to a surface, the gradient of the reflection coefficient is determined by the relationship below:

$$k(\sin(\theta_i) - \sin(\theta_r)) = \frac{d\varphi r(y)}{dy}, \tag{3.15}$$

The local surface phase $r(y)$ and the relationship between i and r are thus given. At each location on the surface, we obtain $r(y)$ by altering the surface impedance. By integrating Snell's equation, we find the necessary phase for the reflection coefficient, which is

$$\varphi_r(y) = -k\sin(\theta_r)y + \sin(\theta_i)y, \tag{3.16}$$

Where: $\varphi_r(y)$ is the required phase at each point y on the metasurface.

Propagation and Pathloss Model: At a random observation angle θ_s, the square of the scattered field magnitude when reflecting a signal in the direction θ_r with an IRS system is:

$$S_{IRS}(r, \theta_s, E_i^2) = \left(\frac{ab}{\lambda}\right)^2 \frac{E_i^2 \cos^2(\theta_i)}{r^2} \left(\frac{\sin\left(\frac{k_0 b}{\lambda}(\sin(\theta_s) - \sin(\theta_r))\right)}{\frac{k_0 b}{\lambda}(\sin(\theta_s) - \sin(\theta_r))} \right)^2, \tag{3.17}$$

this formula describes how the size of the IRS and the angles are used to determine the reflected field magnitude at angle θ_s.

The Pathloss at the far-field distance when a signal is reflected in the direction θ_r by an IRS and expressed as:

$$\beta_{IRS}(r, d_i, \theta_s) = \frac{G_t G_r}{(4\pi)^2} \times \frac{ab}{(d_i d_r)^2} \times \cos^2(\theta_i) \left[\frac{\sin\, y}{y}\right]^2 \tag{3.18}$$

$$y = \frac{k_0 b}{2}(\sin(\theta_s) - \sin(\theta_r)), \tag{3.19}$$

$$\beta_{IRS}(r, d_i, \theta_s) = \frac{G_t G_r}{(4\pi)^2} \times \frac{ab}{(d_i d_r)^2} \times \cos^2(\theta_i) \times \left[\frac{\sin\left(\frac{k_0 b}{\lambda}(\sin(\theta_s) - \sin(\theta_r))\right)}{\frac{k_0 b}{\lambda}(\sin(\theta_s) - \sin(\theta_r))} \right]^2, \tag{3.20}$$

where G_t and G_r are the transmitting and receiving antenna gains, d_i and d_r are the distances from sender to IRS and from IRS to receiver, a and b are the IRS dimensions. θ_r,θ_i, Required angle of incidence and reflection. θ_s, Observation angle. k_0, Wavenumber.

$$\beta_{IRS}(r, d_i, \theta_s) = \frac{G_t G_r}{(4\pi)^2} \times \frac{ab}{(d_i d_r)^2} \times \cos^2(\theta_i), \tag{3.21}$$

this formula represents the path loss when the receiver has $\theta_s = \theta_r$, which is the optimal situation.

3.4 Channel estimation in RIS massive MIMO system

The high dimensionality of cascaded channels and the passive nature of RIS elements pose challenges for channel estimation in RIS-assisted massive MIMO systems. To tackle this issue, advanced compressed sensing techniques leveraging sparsity structures are employed.

Let $h_r \in C^{N\times 1}$ be the channel from user k to the RIS, and $G \in C^{N\times M}$ be the channel between the RIS and the BS (with M antennas). The following provides the cascaded channel [38]

$$H_k = G\ diag(h_{r,k}) \tag{3.22}$$

The channel estimation problem has been converted into a sparse signal recovery problem, and a number of conventional compressed sensing techniques can be used to estimate the sparse signal $\hat{s}$ [43].

$$y = \Phi\hat{s} + n \tag{3.23}$$

3.4.1 Channel Estimation Algorithms

Compressed sensing methods that take advantage of channel sparsity include three primary algorithms:

1. Orthogonal Matching Pursuit (OMP)

The steps of the OMP algorithm are summed up in Algorithm 1. The sparse signal is $\hat{s}$, the sparsity level is K, the observation vector is y, and the initial observation matrix of size $M \times (L+1)$ is Φ [43].

Algorithm 1: Proposed improved OMP algorithm.

1 Initialization parameters : residual $r_0 = y$, index set $\Lambda_0 = \emptyset$, the set of selected column vectors in the observation matrix $A_0 = \emptyset$, and number of iterations $t = 0$.

2 $t = t + 1$, a column α_j of the observation matrix Φ, is searched for the elements that best match the residual according to the principle of maximum correlation, and the index set λ_t is updated, which satisfies the following:

$$\lambda_t = \arg \max_{j=1,2,3,\ldots,N} \left| \left\langle r_{t-1}, \alpha_j \right\rangle \right|$$

3 The index set $\Lambda_t = \Lambda_{t-1} \cup \{\lambda_t\}$ and the set of selected column vectors $A_t = A_{t-1} \cup \alpha\lambda_t$ are updated, where t denotes the current number of iterations and the number of elements in the current index set.

4 The least square solution is found:

$$\widehat{s_t} = \arg \min_s \ \|y - A_t s_t\| = (A_t^H A_t)^{-1} A_t^H y$$

5 New approximations and residuals are calculated: $r_t = y - A_t \hat{s}_t$

6 If $t < K$, the process returns to step 2; otherwise, iteration is stopped and returns to step 7.

7 The non $-$ zero element position set of $\hat{s}$ obtained from the reconstruction is $\Lambda_K = \{\lambda_0, \lambda_1, \ldots \lambda_{K-1}\}$, denotes $\hat{L} = \max(\Lambda_K)$, and the observation matrix $\Phi = \Phi_i'$ and observation vector $y = R_i'$are updated.

8 The set of column vectors of Φ is denoted as $\Phi|_{\Lambda_K}$; with columns indexed using elements in λ_K, the least square solution is found:

$$\hat{s} = \left(\Phi|_{\Lambda_K}{}^H \Phi|_{\Lambda_K} \right)^{-1} \Phi|_{\Lambda_K}{}^H y$$

2. Structured Simultaneous Orthogonal Matching Pursuit (SSOMP)

The steps of the SSOMP algorithm are summed up in Algorithm 2. Step 12 of the SS-OMP (Algorithm 2): CE SS-OMP targets when G_k is constant. The row structure shown in [44] indicates that the sparse channels with the same RIS-BS channel share $\{\Delta p^t_{l_g', l_g}, \Delta q^t_{l_g', l_g}\}$. Therefore, using this functionality to improve the CE process further is justified.

After initialization, there are two main components of SS-OMP.

• **Estimation of $\tilde{h}_1$:** According to stages 2–10, SS-OMP begins by estimating a reference column using OMP. One of the non-zero columns, known as the reference non-zero column $\tilde{h}_1$, is initially recovered using traditional OMP. To estimate the remaining $(L_G - 1)$ non-zero columns, the azimuth and elevation row spacings between the L_f non-zero elements in $\tilde{h}_1$ can be computed using the acquired $\tilde{h}_1$. In particular, step 12 makes it simple to derive the exact spacing vectors Δ_{pr} and Δ_{qr} by using the first estimated non-zero element $h^{1,1}$ in $\tilde{h}_1$ as the reference non-zero element $(l_f' = 1)$. Note that since there are L_f non-zero elements in a single non-zero column, both Δ_{pr} and Δ_{qr} include $(L_f - 1)$ entries.

• **Estimation of the remaining columns by structured shift:** Steps 13–15 of SS-OMP progressively obtain the indices of the non-zero elements in each of the remaining non-zero columns by cyclically adjusting the locations according to $\{\Delta_p^t, \Delta_q^t\}$) after obtaining $\tilde{h}_1$ and the spacings $\{\Delta_p^t, \Delta_q^t\}$)[44].

Algorithm 2: SS-OMP for cascaded CE in the k-th block

Input : $\tilde{\mathbf{Y}}_k, \tilde{\mathbf{W}}_k, \tilde{\Omega}_k, \Delta_p^t, \Delta_q^t, L_G, L_f, M_{G_x}, M_{G_y}$.
Output: $\hat{\tilde{\mathbf{H}}}_k(:, \Omega^c)$

% Initialization
$\hat{\tilde{\mathbf{H}}}_k(:, \Omega^c) = \mathbf{0}_{M_G \times L_G}$
% Estimate the initial non-zero columns via OMP
$\tilde{\mathbf{y}}_1 = \tilde{\mathbf{Y}}_k(:, \Omega^c(1)), \quad \tilde{\mathbf{r}} = \tilde{\mathbf{y}}_1$
for $j = 1$ **to** L_f **do**
  $\mathbf{C} = \text{unvec}_{\{M_{G_x}, M_{G_y}\}}\left(\left|\tilde{\mathbf{W}}_k^{\text{H}} \tilde{\mathbf{r}}\right|\right)$
  $[\mathbf{q}_1(j), \mathbf{p}_1(j)] = \max(\mathbf{C})$
  $\mathbf{s}_1(j) = (\mathbf{p}_1(j) - 1)M_{G_x} + \mathbf{q}_1(j)$
  $\tilde{\mathbf{h}}_1(j) = \tilde{\mathbf{W}}_k(:, \mathbf{s}_1(j))^{\dagger} \tilde{\mathbf{y}}_1$
  $\tilde{\mathbf{r}} = \tilde{\mathbf{y}}_1 - \tilde{\mathbf{W}}_k(:, \mathbf{s}_1(j)) \tilde{\mathbf{h}}_1(j)$
end for
$\hat{\tilde{\mathbf{H}}}_k(\mathbf{s}_1, \Omega^c(1)) = \tilde{\mathbf{h}}_1$
% Estimate the remaining non-zero columns exploiting row-structure B
for $l = 2$ **to** L_G **do**
  $\tilde{\mathbf{y}}_l = \tilde{\mathbf{Y}}_k(:, \Omega^c(l))$
  %Obtain the indices of the non-zero elements in each non-zero column.
  for $i = 1$ **to** L_f **do**
    $\mathbf{p}_l(i) = \text{circ}[\mathbf{p}_1(i), \Delta\mathbf{p}^t(l-1)]M_{G_x}$
    $\mathbf{q}_l(i) = \text{circ}[\mathbf{q}_1(i), \Delta\mathbf{q}^t(l-1)]M_{G_y}$
  end for
  $\mathbf{s}_l = (\mathbf{p}_l - 1)M_{G_x} + \mathbf{q}_l$
  $\tilde{\mathbf{h}}_l = \tilde{\mathbf{W}}_k(:, \mathbf{s}_l)^{\dagger} \tilde{\mathbf{y}}_l$
  $\hat{\tilde{\mathbf{H}}}_k(\mathbf{s}_l, \Omega^c(l)) = \tilde{\mathbf{h}}_l$
end for

3. Double-Structured Orthogonal Matching Pursuit (DSOMP)

The steps of the DSOMP algorithm are summed up in Algorithm 3.The following is an explanation of the primary steps involved in Algorithm 3.
In Step 1, we employ row-structured sparsity to jointly estimate the common row support, referred to as Ω_r. This support includes L_G row indexes associated with L_G non-zero rows.
Moving to Step 2, we utilize partially column-structured sparsity to estimate further

the partially common column support, labeled as $\Omega_c^{l_1,Com}$ non-zero row.
Step 3 focuses on the individual estimation of user-specific column supports for each user k.
Steps 4 through 8 involve using the least squares (LS) technique to derive the estimated matrices $\left\{\hat{\tilde{H}}\right\}_{k=1}^{K}$, after detecting the supports of all the sparse matrices.
Notably, the sparse signal is $\tilde{H}_k^H$, while the sparse matrix calculated through the LS method in Step 6 is $\hat{\tilde{H}}_k^H$.
Finally, in Step 9, by converting angular channels into spatial channels, we obtain the estimated cascaded channels $\{\widehat{H}_K\}_{k=1}^K$ [38].

Algorithm 3: DS-OMP Based Cascaded Channel Estimation

Input : $\tilde{\mathbf{Y}}_k$: $\forall k$, $\tilde{\Theta}$, L_G, $L_{r,k}$:, $\forall k$, L_c.
Initialization: $\hat{\tilde{\mathbf{H}}}_k = \mathbf{0}_{M\times N}$, $\forall k$
Stage 1: Return estimated completely common row support $\widehat{\Omega}_r$ by Algorithm 2.
Stage 2: Return estimated partially common column supports $\left\{\widehat{\Omega}_c^{l_1,Com}\right\}_{l_1=1}^{L_G}$ based on $\widehat{\Omega}_r$ by Algorithm 3.
Stage 3: Return estimated column supports $\left\{\left\{\widehat{\Omega}_c^{l_1,k}\right\}_{l_1=1}^{L_G}\right\}_{k=1}^{K}$ based on $\widehat{\Omega}_r$ and $\left\{\widehat{\Omega}_c^{l_1,Com}\right\}_{l_1=1}^{L_G}$ by Algorithm 4.
for $l_1 = 1, 2, \ldots, L_G$ **do**
  for $k = 1, 2, \ldots, K$ **do**
    $\hat{\tilde{\mathbf{H}}}_k^H(\hat{\Omega}_c^{l_1,k}, \hat{\Omega}_r(l_1)) = \tilde{\Theta}^{\dagger}(:, \hat{\Omega}_c^{l_1,k}) \cdot \tilde{\mathbf{Y}}_k(:, \hat{\Omega}_r(l_1))$
  end for
end for
$\hat{\mathbf{H}}_k = \mathbf{U}_M^H \cdot \hat{\tilde{\mathbf{H}}}_k \cdot \mathbf{U}_N$, $\forall k$
Output: Estimated cascaded channel matrices $\widehat{H}_k$, $\forall k$.

As the performance statistic, we employ the normalized mean square error (NMSE), which is provided as [45]:

$$NMSE = E\left[\frac{\|\widehat{H}_k - H_k\|_2^2}{\|H_k\|_2^2}\right] \tag{3.24}$$

3.5 Simulation Examples and discussion

3.5.1 Example 1

This example uses the $3GPP$ Urban Micro (UMi) channel model to compare gains from the two conditions that are typical of LOS and NLOS at a carrier frequency of $3GHz$, ignoring shadow fading in order to create a deterministic model. Antenna gain for both transmitter and receiver is set to $G_t = G_r = 5dB_i$ Channel gain is evaluated as a function of distance between transmitter and receiver for distances $> 10m$ considered

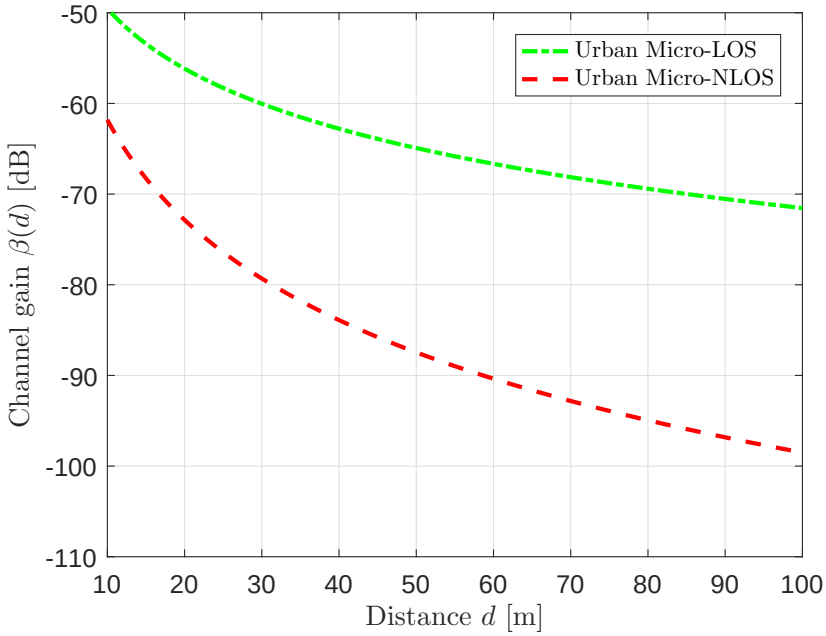

Figure 3.2: Typical channel gains as a function of the distance, when including the antenna gains $G_t = G_r = 5dB_i$.

Figure 3.2 illustrates how distance impacts channel gain, showing that LOS conditions yield better performance than NLOS conditions. A channel gain value of $60dB$ indicates a significant improvement compared to typical values, which range from $70dB$ to $110dB$. The findings suggest that using NLOS paths can result in considerable performance degradation, especially in urban areas where buildings and other obstacles obstruct direct lines of sight. This underscores the need for supportive technologies, such as IRS or relays, which can establish alternative paths that enhance channel conditions.

3.5.2 Example 2

This example compares the required transmit power to achieve data rates of $\overline{R} = 4bit/s/Hz$ and $\overline{R} = 6bit/s/Hz$ using three systems: regular SISO, DF relaying, and IRS with 25, 50, 100,150 reflecting elements. The configuration considers a bandwidth of $10MHz$, a noise power level of $-94dBm$, an amplitude reflection coefficient of $\alpha = 1$, the distances of $d_{sr} = 80m$ from the source to the relay/IRS and $d_{rd} = 10m$ from the relay/IRS to the destination.

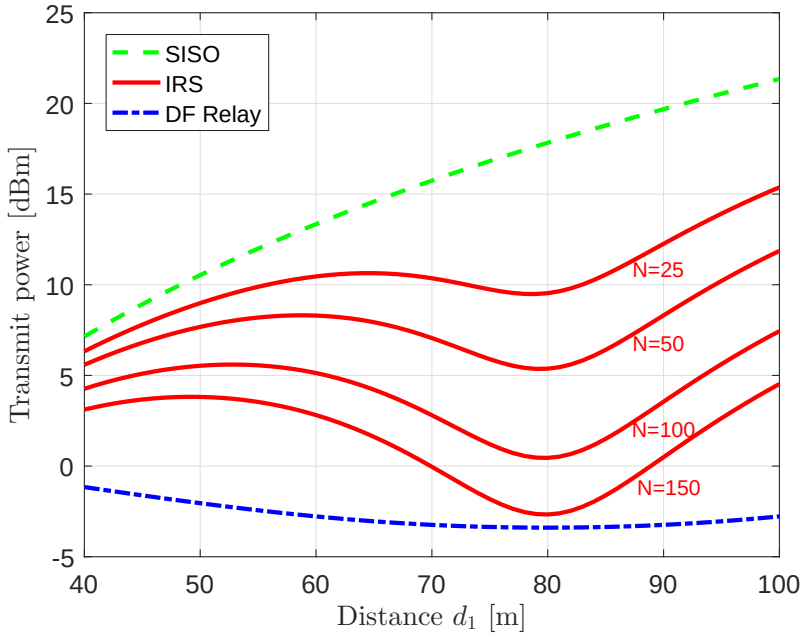

Figure 3.3: The transmit power needed to achieve the rate $\overline{R} = 4bit/s/Hz$

.

In a scenario where the transmission rate is $\overline{R} = 4bit/s/Hz$, Figure 3.3 illustrates that the basic SISO system requires the highest transmission power. This is due to the lack of external signal enhancement, which necessitates a significant amount of energy to maintain signal quality. In contrast, the DF relaying system uses the least amount of power among all the configurations examined, as it effectively retransmits signals, thereby minimizing energy loss.

The IRS-assisted system's transmission power needs reduce as the number of IRS elements N rises because intelligent reflections improve the SINR, which boosts system efficiency. However, the performance difference between IRS and DF relaying is negligible when the receiver is near the IRS or the source, since fewer IRS reflections are required to improve the signal. The number of IRS elements must exceed 164 at $d_1 = 80m$ to guarantee that performance exceeds DF Relaying.

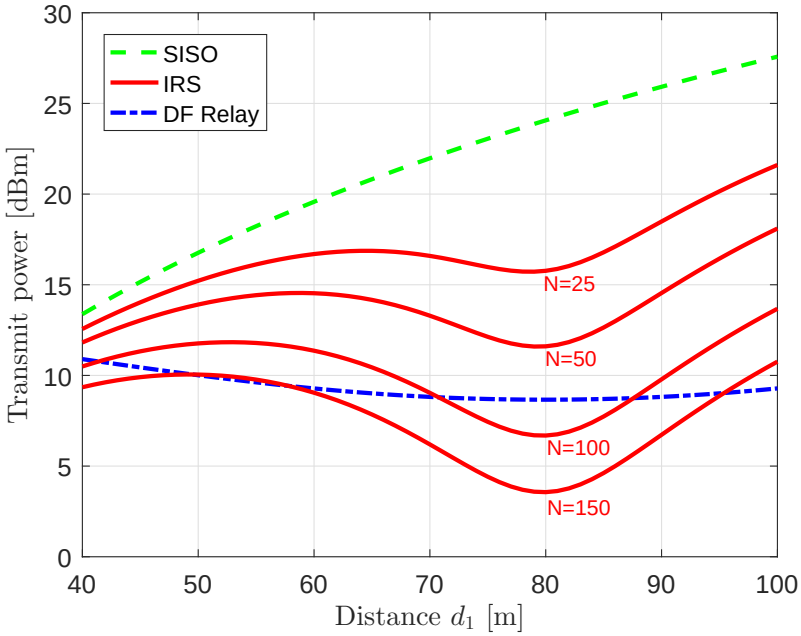

Figure 3.4: The transmit power needed to achieve the rate $\overline{R} = 6bit/s/Hz$.

Figure 3.4 illustrates the relationship between transmission rate and power consumption. As the transmission rate $(\overline{R})$ increases to $6bits/s/Hz$, the required transmit power also rises. However, the potential of IRS-assisted communication to reduce power requirements makes it more competitive when the target is located close to the source. To exceed the performance of DF relaying, an IRS with more than 76 elements is sufficient when the distance (d_1) is $80meters$. This requirement arises because DF relaying's spectral efficiency is limited by a 1/2 Prelog factor penalty. In contrast to IRS systems, where optimized reflection topologies mitigate these increases, the necessary SINR and thus the transmit power-grows more sharply with the transmission rate in DF relaying.

3.5.3 Example 3

Analyzing the energy efficiency of SISO, DF relay, and IRS-based systems. The analysis assumes the following parameters: the power consumption at the source, destination, and relay is $P_s = P_d = P_r = 100mW$; the IRS element power is $P_e = 5mW$; and the fixed distance is $d_1 = 70m$, where $\mathbf{V} = 0.5$.

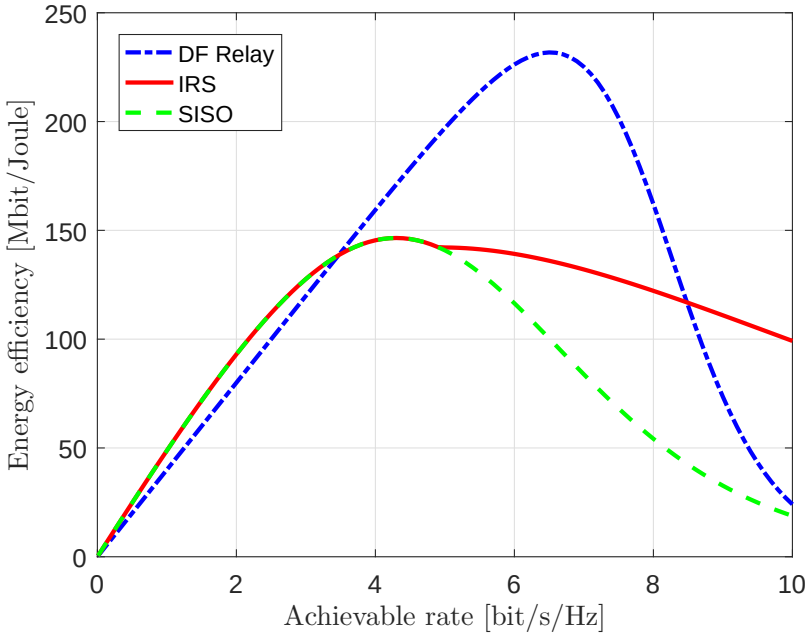

Figure 3.5: The energy efficiency as a function of the rate $\overline{R}$.

Figure 3.5 shows how energy efficiency (EE) and data rate $(\overline{R})$ are related. To maximize efficiency, the number of IRS pieces is chosen for each $\overline{R}$. Based on the findings in the figure:

The SISO system's simplicity and low power consumption allow it to achieve the best energy efficiency at low data rates $\overline{R} \leq 0.347 bit/s/Hz$.

Since DF relaying efficiently boosts the signal and lowers power consumption, it operates better in the range $\overline{R} \in (3.47, 8.48] bit/s/Hz$.

When $N_{opt} > 0$, the influence of IRS becomes apparent at $\overline{R} > 4.9 bit/s/Hz$, underscoring the crucial role that IRS components play in performance enhancement. Additionally, the figure demonstrates that IRS outperforms DF relaying at $\overline{R} > 8.48 bit/s/Hz$, thanks to clever signal reflections that lower the transmission power needed for high data rates and improve the signal-to-noise ratio.

Thus, transitioning from a SISO to a DF relaying setup is more advantageous for reducing power consumption and enhancing energy efficiency, except when extremely high rates are required.

3.5.4 Example 4

In this example, we simulate the reflected (scattered) electromagnetic field intensity on a flat metal surface at different sizes and viewing angles θ_s at a standing wave angle of incidence $\theta_s = 30°$ We analyze the beamwidth as a function of the surface dimensions

compared to the wavelength. We assume a wave frequency $f = 3GHz$, a wavelength $\lambda = c/f = 0.1m$, and a rectangular surface with dimensions $a \times b$. We also consider three cases with different sizes: $a = b = 0.2\lambda, \lambda$ and 10λ.

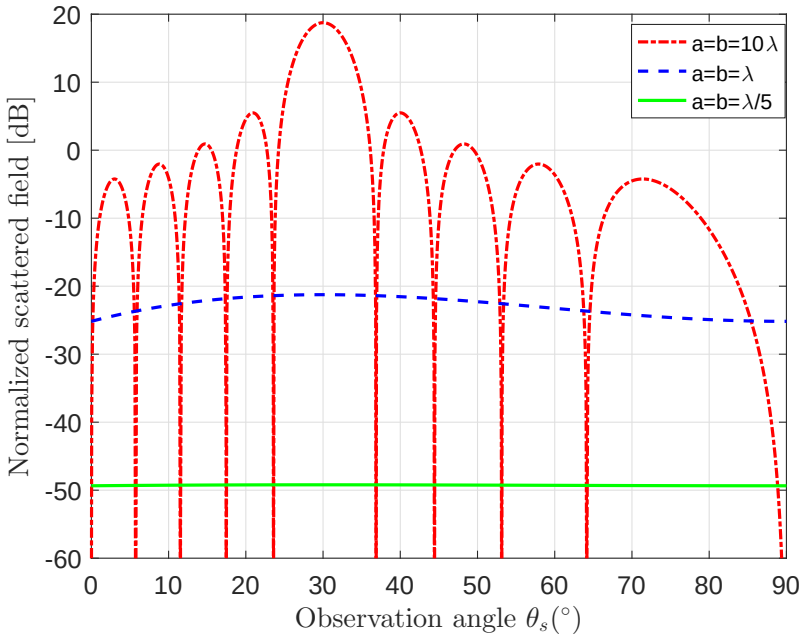

Figure 3.6: Normalized squared magnitude of the scattered field as a function of the angles θ_s where $\theta_i = 30$

The results indicate that the reflected radiation pattern becomes more directional as the physical size of the reflecting surface increases. In particular, the reflected energy is mostly concentrated around the specular reflection angle $\theta_s = \theta_i$, where $a = b = 10\lambda$. This results in a narrow beam around $\theta_s = 30°$, where the main lobe is sharp and has several side lobes. This indicates that most of the energy is reflected in a single direction by the plate. In contrast, smaller surfaces (such as $a = b = \lambda$ or $\lambda/5$) show diffuse reflection in different directions, a more diffuse field, and larger radiation patterns with lower peak intensity.

3.5.5 Example 5

Consider a scenario in which an incident electromagnetic wave, θ_i, is redirected to different reflection angles, θ_r, and its corresponding y-divergence at the central origin is achieved by changing the local phase of its components on an IRS. These parameters define the system we are studying here: The carrier frequency is $3GHz$, the wavelength is $\lambda = 0.1m$, the angle of incidence is $\theta_i = 30°$, and the wavenumber is $k_0 = 2\pi/\lambda$. The dimensions of the square IRS surface are: $a = b \in 0.2\lambda, \lambda, 10\lambda$ and 16λ is the y-axis

length.

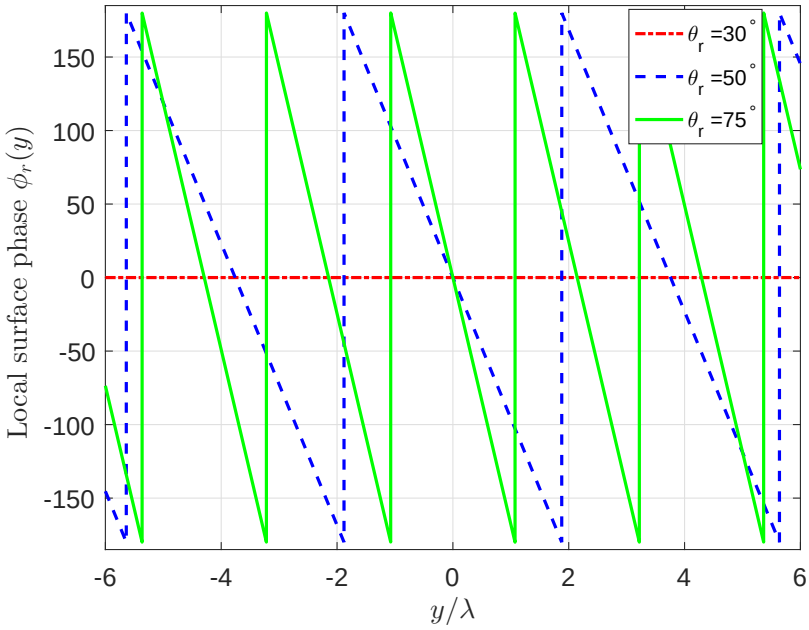

Figure 3.7: Local surface phase that is required to redirect the incident wave with $\theta_i = 30$ in a desired direction θ_r.

Figure 3.7 shows the phase (y) required to transmit the reflected wave at three angles: 30°, 50°, and 75°. We used Snell's generalized law in the calculation, which allows us to control unusual reflections. In this figure, the y/λ axis shows where we are on the IRS surface at lambda wavelengths. The y-axis shows the desired local phase at each point y, in degrees from -180 to $+180$. The red line in the figure shows when the reflection angle is the same as the incidence angle, $\theta_i = \theta_r$. Here, the phase is constant across the surface, meaning there is no phase change. When $\theta_r \neq \theta_i$, the phase changes gradually along the surface. That is, as the reflection angle moves away from the incidence angle, the phase gradient becomes larger and faster. The dark line also gives an example at a larger reflection angle: $\theta_r = 75$ *degree*.

3.5.6 Example 6

In this example, an IRS operating at a frequency $f = 3GHz$, and a wavelength $\lambda = 0.1m$, is used to study how phase quantization affects reflection accuracy. The reflected signal is oriented at an angle of $\theta_r = 75°$, while the angle of incidence $\theta_i = 0°$. Although the Snell equation determines the reflection phase at each point on the surface, a continuous phase cannot be produced with infinite precision in science. As a result, this phase is quantized into a small number of levels. 3-bit quantization, or $3^2 = 8$ phase

levels, is used.

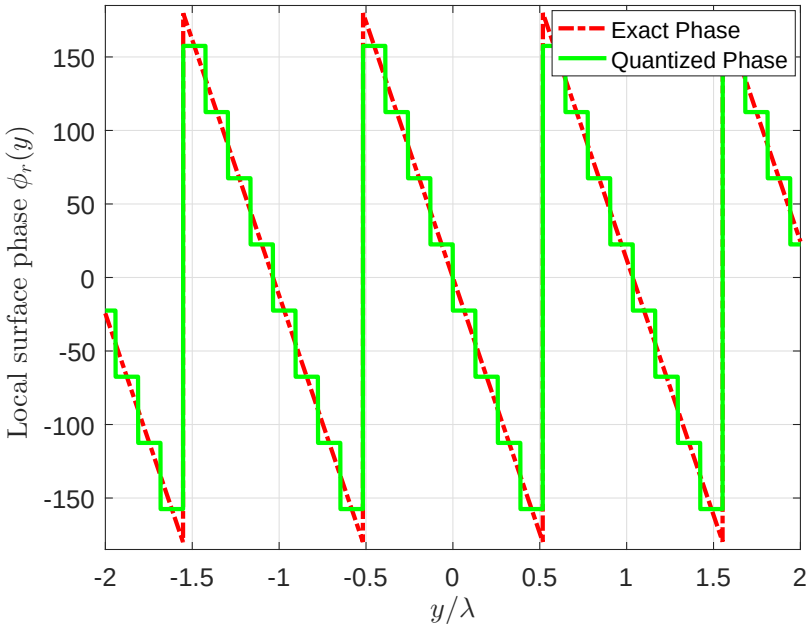

Figure 3.8: The quantized local surface phase that is required to redirect the incident wave with $\theta_i = 0$ to $\theta_r = 75$.

Figure 3.8 shows how the phase can be quantized into discrete phases, where the required step size would be $\lambda/5$. This divides the surface into tiny segments, each containing a solid phase. The smaller these segments are, the more accurate the phase approximation that is required. However, with greater accuracy, a design becomes much more complicated, and there will be interference issues between elements. If the elements are too big, then the local phase will be approximated. This causes a mismatch between the required reflection angle and what is measured at the surface. As seen from the difference that appears between the quantized distribution and the ideal phase distribution, quantization creates a phase divergence between the ideal and real phases, which little divergence reflects.

3.5.7 Example 7

In this example, we examine the effect of the size of the IRS on path loss as a function of the observation angle θ_s and the distance between the surface and the receiver. The minimum is achieved when $\theta_s = \theta_r$, i.e., when the receiver and transmitter are at the same distance from the IRS, the angle is optimal. We also focus on the effect of scattering. The surface uses an incoming signal with an incidence angle of $\theta_s = 30°$, and the required angle for signal reflection is $\theta_s = 60°$. The two antennas have equal

gain for both transmitter and receiver, where $G_t = G_r = 5dB$, and the distances $d_t = 50$ and $d_r = 25m$.

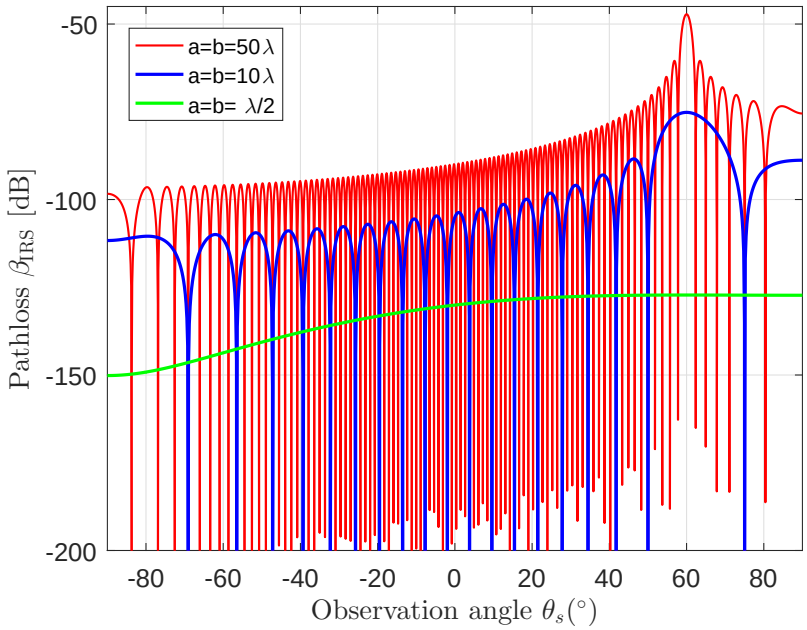

Figure 3.9: The Pathloss of the reflected path. The angles are $\theta_i = 30$ and $\theta_r = 60$ where the antenna gains are $G_t = G_r = 5dB$, the distances are $d_i = 50$ and $r = 25$ *meters*.

The results show that as the surface size increases (for example, $a = b = 50\lambda$), as shown by the red line, we observe a very sharp peak at angle $\theta_s = 60°$, which is the required steering angle θ_r. This indicates that the reflected beam is more focused and has a narrow beamwidth and angular direction. At other angles, very weak signals (with significant loss) are observed. For medium magnitude ($a = b = 10\lambda$), shown by the blue line, there is a peak at 60°, but it is slightly weaker and wider than at 50λ. This means that the beam is still directed, but not as focused and precise, and loses its ability to direct the signal. When magnitude is small (e.g., $a = b = \lambda/2$), shown by the green line, we observe a flattened curve, indicating that the surface appears randomly scattered, causing the signal to spread in multiple directions without a clear direction.

3.5.8 Example 8

This simulation aims to evaluate and compare the performance of different channel estimation algorithms for a reconfigurable RIS wireless communication system. We investigate several compressive sensing-based channel estimation algorithms (Oracle LS, OMP, SS-OMP, and DS-OMP) for a smart surface-based wireless system. The system features a 64-antenna BS, a 256- elements RIS, and 16 users, with fixed BS-RIS distances

of $10m$ and $100m$ between users and the RIS. The simulation models sparse channels with a fixed number of paths (5 BS-RIS paths and 8 RIS user paths, including 4 common paths) and uses 64 experimental transmissions for estimation. The SNR range (from $-10dB$ to $20dB$) is used to evaluate the algorithm's performance.

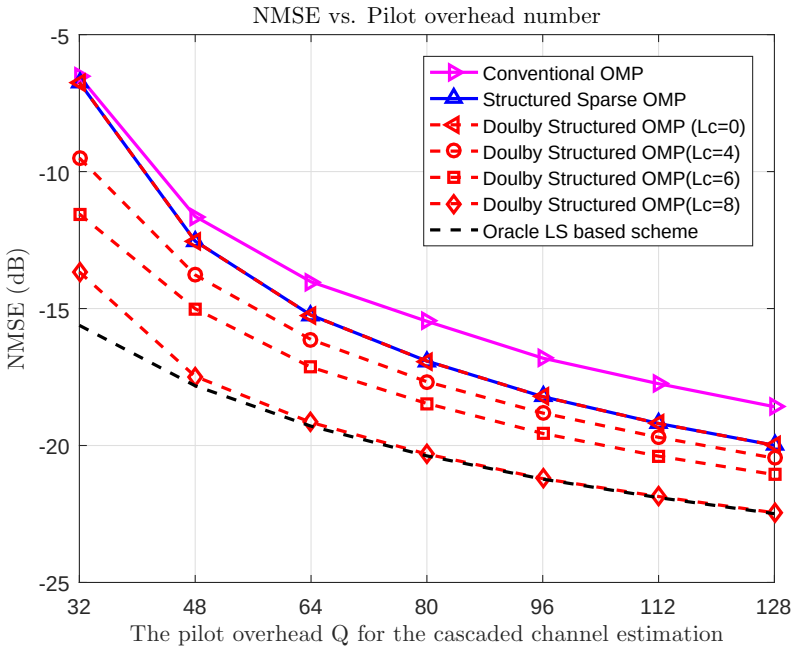

Figure 3.10: NMSE performance comparison against the pilot overhead Q

Figure 3.10 displays the relationship between the NMSE and the number of pilot signals (Q) used in channel estimation under an IRS system. It shows that in the absence of common paths ($L_c = 0$), the DS-OMP achieves an estimation accuracy comparable to that of the SS-OMP. This observation confirms the effectiveness of the transition from a double-structured model to a sparse queue-based model. As the number of common paths between the users and the IRS increases, specifically at ($L_c = 4$, $L_c = 6$, and $L_c = 8$), the accuracy of the DS-OMP pursuit approaches that of the Oracle LS system. This system enhances communication quality and incremental improvements to the performance of RISs by reducing pilot signals and supporting more accurate channel estimation.

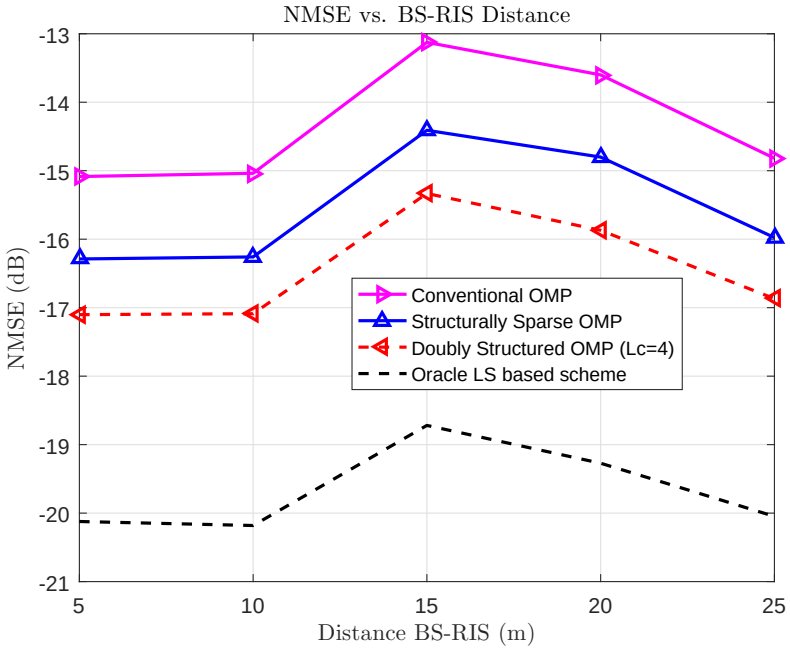

Figure 3.11: Effect of the BS-RIS distance on the NMSE.

This Figure 3.11 shows how the distance between the BS and RIS affects the NMSE, pointing out how well different methods for estimating channels work. As this distance grows, the NMSE gets worse; path loss weakens the received signal and lowers its SNR, against which noise hampers accurate channel estimation. Of all the methods compared, the standard OMP algorithm is most sensitive to path loss since its NMSE increases so steeply with distance.

This shows its small ability to deal with places that have high weakening, and it's not using the built-in features of the path. Structurally Sparse OMP presents modest improvements in performance through the exploitation of row-wise sparsity, which relates to the correlation among the antenna elements; however, it continues to suffer degradation as the distance increases, though to a lesser degree. The proposed DS-OMP ($L_c = 4$) offers superior estimation performance at all measured distances since it exploits both row and column sparsity, capturing spatial and angular characteristics of RIS-assisted channels, hence, structural aspects inherently provide robustness against signal degradation with distance and maintain a consistently lower NMSE than all other practical algorithms. Oracle LS-based scheme achieves the lowest NMSE in all cases; however, it is meant for benchmarking purposes since its dependence on perfect CSI precludes its use in practice.

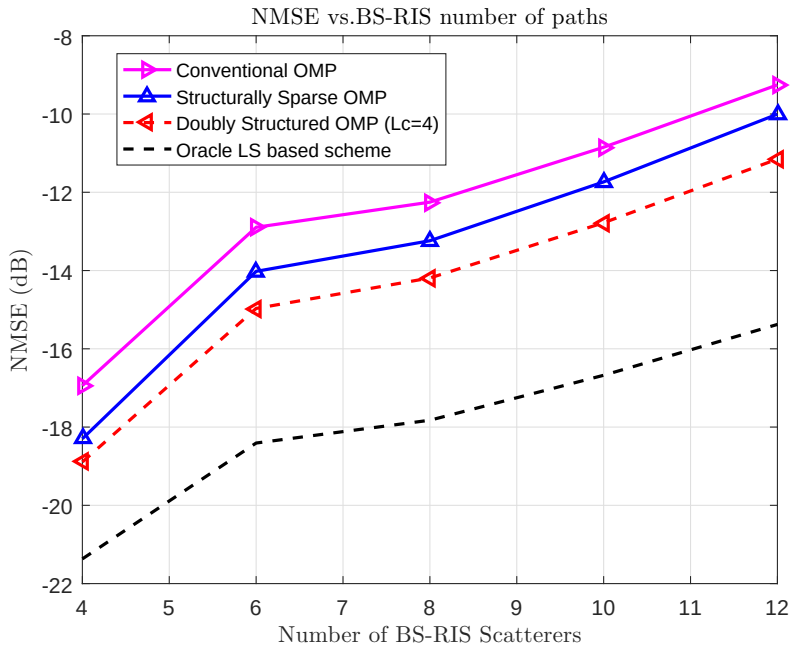

Figure 3.12: Effect of the number of scatterers between the BS and the RIS on the NMSE.

This graph shows the relationship between the number of scatterers in the space between the RIS and the BS versus the mean NMSE. Increasing the number of scatterers has fairly much degraded all algorithms. This results in a closing gap in algorithm performance and a giant increase in the value of the mean normalized squared error. The reason is that increasing paths results in a more complex channel model, hence, estimation errors become more probable, especially when both routing signals and SNR are constrained.

Since the conventional OMP algorithm does not take into account the scattering of the channel structure, it has been by far the worst-performing algorithm in a comparison of algorithms. When the number of paths is limited, the SS-OMP algorithm exploits the partially scattered structure to realize average performance. Regarding other methods, the DS-OMP algorithm performs better, particularly when there are few scatterers. This superiority reflects that the algorithm can exploit characteristics offered by the dual-channel architecture (time and space scarcity) for more accurate and efficient estimation in resource-constrained contexts. The Oracle LS algorithm outperforms all other algorithms since it knows the path locations a priori.

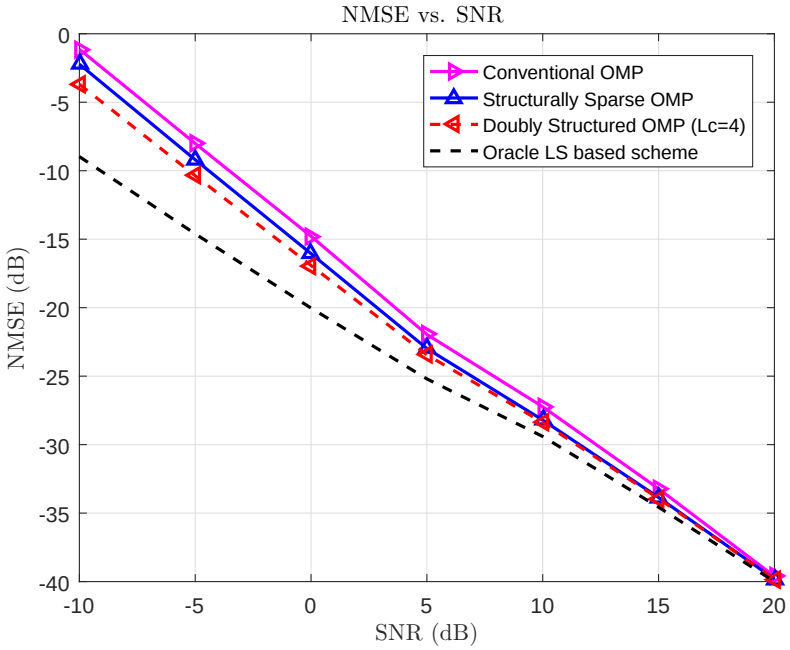

Figure 3.13: Effect of the signal to noise ratio on the NMSE.

The effect of SNR, which ranges from -10 to $20dB$, on the NMSE for a collection of distinct algorithms is shown in Figure 3.13. As noise becomes less of an influence, an increase in SNR results in a decrease in NMSE, suggesting increased estimation accuracy. Better algorithm performance and more accurate identification of the partially common column support are linked to larger values of L_c. The NMSE is comparatively large at $-10dB$, and at low SNRs like $-5dB$, the performance of SS-OMP and Conventional OMP drastically deteriorates.

Because of the dual nature of the support across both rows and columns, the DS-OMP algorithm ($L_c = 4$) performs better than the other algorithms and selects columns more effectively during estimate. Its performance is quite similar to that of Oracle LS, suggesting that it can accurately determine cross-column support even in the absence of the prior knowledge that Oracle LS has.

As demonstrated by the close alignment of both curves, the overlap between the DS-OMP and SS-OMP curves at high SNR values further indicates that the dual structure simplifies to a purely row-based structure when $L_c = 0$. Note: Oracle LS is a theoretical benchmark that reflects the optimal minimal estimate error and represents the best performance possible when the true channel support is known.

3.6 Conclusion

In this chapter, the performance of wireless communication systems, SISO, IRS, and advanced relay (DF) techniques were analyzed using mathematical modelling and numerical simulation. Results show that energy efficiency improves with IRS along with channel estimation and also reduces path loss, especially with increasing the number of reflective elements and in high-dispersion environments. The DF techniques proved efficient under effective specific conditions, but are limited as the relay distance increases. It was also shown that the path loss modelling by physical optics techniques, and that increasing the size of the IRS increases the directivity of the signal. On the other hand, increasing phase loss decreases reflection accuracy. The DS-OMP algorithms proved to be very accurate in estimation and performed very well in dealing with weak channels.

General Conclusion

The significance of incorporating IRS into huge MIMO systems is discussed in this research. This work has helped us understand how this technology can significantly improve signal quality, decrease interference, and increase spectrum efficiency particularly in complicated surroundings where direct line-of-sight is impossible. Additionally, we offer a thorough analysis of IRS technology, going over the distinctions between passive and active IRS models and contrasting their effectiveness with that of conventional relay systems. By altering the phase at each reflective part, we show how it may intelligently regulate electromagnetic wave propagation, enhancing signal quality and lowering interference. After that, we run performance analysis and simulations.

We draw the conclusion that future wireless communications networks can incorporate and use IRS technology. We suggest the DS-OMP algorithm as a practical way to estimate channels effectively. The outcomes show notable improvements in several areas, most notably energy and spectrum efficiency. According to the study's findings, smart reflective surfaces are a paradigm change in smart wireless network design, and their successful integration with massive MIMO is an essential first step and one of the most promising approaches for the creation of 6G networks.

Bibliography

[1] Chataut, Robin, and Robert Akl. *"Massive MIMO systems for 5G and beyond networksoverview, recent trends, challenges, and future research direction."* Sensors 20.10 (2020): 2753

[2] Payaswini, P., and D. H. Manjaiah. *"Challenges and issues in 4g networks mobility management."* arXiv preprint arXiv:1402.3985 (2014).

[3] MAIFIA Khalil, BOUZIANE Badre Eddine, «*CODAGE ET TRANSMISSION DE L'INFORMATION : CAS DU RESEAU RADIO-MOBILE 4G*», Mémoire de Fin d'Etude, Université 8 Mai 1945 – Guelma 2019.

[4] Lim, Chaiman, et al. *"Recent trend of multiuser MIMO in LTE-advanced."* IEEE Communications Magazine 51.3 (2013): 127-135.

[5] Aounallah, N., ADILA Manel et KAFI Kaoutar, « *Performances des algorithmes d'estimation du canal pour un système MIMO massif*» , Mémoire de Fin d'Etude, Université Kasdi Merbah Ouargla, 2019.

[6] Sun, Shu, et al. *"MIMO for millimeter-wave wireless communications: Beamforming, spatial multiplexing, or both?"* IEEE Communications 52.12 (2014): 110-121

[7] Abdelhay, E. H., et al. *"Spatial Diversity and Multiplexing Effects on Uplink Multi-hop LTE-Advanced."* MEJ-Mansoura Engineering Journal 40.2 (2020): 12-21.

[8] Aounallah, N., Boufadi Fatima Zahra et kanouri Manal, «*Analysis study of different precoding schemes for massive MIMO system*» , Mémoire de Fin d'Etude, Université Kasdi Merbah Ouargla, 2021.

[9] Heba Soffar, *"5G network features, uses, importance, dangers, What is 5g technology & How it works?,"*page de web, 9 Mars 2019.

[10] Detti, Andrea. *"Functional architecture."* 5G Italy White Book: From Research to Market, CNIT (2018): 59-68.

[11] Abdel Ghaffar, Aziz, et al. *"Modeling and Evaluation of Software-Defined Networks Based on 5G Core Network Architecture."* IEEE Access 9 (2021): 10179-10198.

[12] Chittimoju, Gayatri, and Usha Devi Yalavarthi. *"A comprehensive review on millimeter waves applications and antennas."* Journal of Physics: Conference Series. Vol. 1804. No. 1. IOP Publishing, (2021).

[13] Filgueiras, Hugo Rodrigues Dias, et al, *"Wireless and optical convergent access technologies toward 6G"*, IEEE Access 11 (2023): 9232-9259.

[14] Mem. GUEBGOUB NASSIMA., ALLEL MONCEF, AMRAOUI ZAKARI, «*Conception de nouveau système d'antennes MIMO pour le standard 5G*», Mémoire de Fin d'Etude, Université 8 Mai 1945 – Guelma (2021).

[15] Lu, Lu, et al. *"An overview of massive MIMO: Benefits and challenges."* IEEE journal of selected topics in signal processing 8.5 (2014): 742-758.

[16] Albreem, Mahmoud A., Marco Gonti, and Shahryar Shahabuddin, *"Massive MIMO Detection Techniques: A Survey."* IEEE Communications Surveys & Tutorials 21.4 (2019): 3109-3132.

[17] Aounallah, N., BOUHAFSMERIEM et BLAL AMA, «*Analysis study of different precoding schemes for massive MIMO system*» , Mémoire de Fin d'Etude, Université Kasdi Merbah Ouargla, (2021).

[18] Gkagkas, Georgios, et al, *"The Advantage of the 5G Network for Enhancing the Internet of Things and the Evolution of the 6G Network."* Sensors 24.8 (2024): 2455.

[19] Serghiou, Demos, et al, *"Terahertz channel propagation phenomena, measurement techniques and modeling for 6G wireless communication applications: A survey, open challenges and future research directions"*, IEEE Communications Surveys & Tutorials 24.4 (2022): 1957-1996.

[20] Liu Sun, Li Zhao* and Rui-Yun Peng*, « *Research progress in the effects of terahertz waves on biomacromolecules*», (2021)

[21] Al-Saadi, Wajdan K., et al, *"Spectrum Options and Allocations for 6G: A Regulatory and Standards Review "*, Journal of the IEEE Open Communications Society, Vol. 4 (2023): 1787–1812.

[22] Feng, Rui, et al, *"Recent Advances of 6G Ultra-Massive MIMO Technologies in Spatial and Beam Domains"* arXiv preprint arXiv:2501.10429 (2025).

[23] Aounallah, N.et LABED Smail, Yahiaoui Abir et Zegrir Ilham, «*Study of the impact of very large-scale antennas on improving the performance of 5 and 6G wireless mobile networks*» , Mémoire de Fin d'Etude, Université Kasdi Merbah Ouargla, (2023).

[24] K. Vaigandla and D. N. Venu, "*Survey on massive mimo: Technology, challenges, opportunities and benefits*", (2021).

[25] Kumar, Arun, et al, *"Implementation of the deep learning method for signal detection in massive-MIMO-NOMA systems"*, Heliyon 10.3 (2024).

[26] Labed, Smail, and Naceur Aounallah, *"Efficient Iterative Detection Based on Conjugate Gradient and Successive Over-Relaxation Methods for Uplink Massive MIMO Systems"* Journal of Telecommunications and Information Technology 2 (2023).

[27] Albreem, Mahmoud A., et al, *"Overview of precoding techniques for massive MIMO"*, Ieee Access 9 (2021): 60764-60801

[28] Mucchi, Lorenzo, et al, *"Signal processing techniques for 6G"*, Journal of Signal Processing Systems 95.4 (2023): 435-457

[29] Vilas Boas, Evandro C., et al, *"Artificial intelligence for channel estimation in multicarrier systems for B5G/6G communications: A survey"*, EURASIP Journal on Wireless Communications and Networking 2022.1 (2022): 116.

[30] Pan, Cunhua, et al, *"Reconfigurable intelligent surfaces for 6G systems: Principles, applications, and research directions."* IEEE Communications Magazine 59.6 (2021): 14-20.

[31] *"Reconfigurable intelligent surfaces for 6G systems: Principles, applications, and research directions."*

[32] Kang, Zhenyu, Changsheng You, and Rui Zhang. *"Active-passive IRS aided wireless communication: New hybrid architecture and elements allocation optimization."* IEEE Transactions on Wireless Communications 23.4 (2023): 3450-3464.

[33] Perez-Adan, Darian, et al. *"Intelligent reflective surfaces for wireless networks: An overview of applications, approached issues, and open problems."* Electronics 10.19 (2021): 2345.

[34] Okogbaa, Fred Chimzi, et al. *"Design and application of intelligent reflecting surface (IRS) for beyond 5G wireless networks: A review."* Sensors 22.7 (2022): 2436.

[35] Zhang, Zijian, and Linglong Dai. *"Reconfigurable intelligent surfaces for 6G: Nine fundamental issues and one critical problem."* Tsinghua Science and Technology 28.5 (2023): 929-939.

[36] Gong, Shimin, et al. *"Toward smart wireless communications via intelligent reflecting surfaces: A contemporary survey."* IEEE Communications Surveys & Tutorials 22.4 (2020): 2283-2314.

[37] Swindlehurst, A. Lee, et al. *"Channel Estimation with Reconfigurable Intelligent Surfaces–A General Framework."* arXiv preprint arXiv:2110.00553 (2021).

[38] Wei, Xiuhong, Decai Shen, and Linglong Dai. *"Channel estimation for RIS assisted wireless communications—Part II: An improved solution based on double-structured sparsity."* IEEE Communications Letters 25.5 (2021): 1403-1407.

[39] Li, Bo, et al. *"Robust sensing matrix design for the Orthogonal Matching Pursuit algorithm in compressive sensing."* Signal Processing 227 (2025): 109684.

[40] Determe, Jean-François, et al. *"On the exact recovery condition of simultaneous orthogonal matching pursuit."* IEEE Signal Processing Letters 23.1 (2015): 164-168.

[41] Björnson, Emil, Özgecan Özdogan, and Erik G. Larsson. *"Intelligent reflecting surface versus decode-and-forward: How large surfaces are needed to beat relaying?."* IEEE wireless communications letters 9.2 (2019): 244-248.

[42] Özdogan, Özgecan, Emil Björnson, and Erik G. Larsson. *"Intelligent reflecting surfaces: Physics, propagation, and pathloss modeling."* IEEE Wireless Communications Letters 9.5 (2019): 581-585.

[43] Si, Lu, et al. *"An improved orthogonal matching pursuit algorithm for cs-based channel estimation."* Sensors 23.23 (2023): 9509.

[44] You, You, et al. *"Adaptive Channel Estimation for RIS-Assisted Systems in Time-Varying mmWave Channels."* IEEE Transactions on Communications (2024).

[45] Chen, Jie, et al. *"Channel estimation for reconfigurable intelligent surface aided multi-user mmWave MIMO systems."* IEEE Transactions on Wireless Communications 22.10 (2023): .6853-6869